SIMULATION OF A COLD-AIR POOL IN UTAH'S SALT LAKE VALLEY

by

Christopher Stephen Foster

A thesis submitted to the faculty of
The University of Utah
in partial fulfillment of the requirements for the degree of

Master of Science

Department of Atmospheric Sciences

The University of Utah

December 2015

The University of Utah Graduate School

STATEMENT OF THESIS APPROVAL

The thesis of **Christopher Stephen Foster**

has been approved by the following supervisory committee members:

John D. Horel	, Chair	**October 5, 2015** Date Approved
John Chun-Han Lin	, Member	**October 5, 2015** Date Approved
Sebastian Wilhelm Hoch	, Member	**October 5, 2015** Date Approved

and by **Kevin D. Perry** , Chair/Dean of

the Department/College/School of **Atmospheric Science**

and by David B. Kieda, Dean of The Graduate School.

ABSTRACT

The Persistent Cold-Air Pool Study (PCAPS), which took place in Utah's Salt Lake Valley during winter 2010-2011, provides a rich dataset of targeted observations at scales appropriate for better understanding the dynamical evolution of persistent cold-air pools. We examine the influence of the land use and land cover datasets available within the Weather Research and Forecasting (WRF) numerical model on the model's ability to accurately simulate a persistent cold-air pool (CAP). A modified version of the most recently released land use dataset, 2011's National Land Cover Database (NLCD 2011), was used to model a CAP that occurred from 1 January 2011 to 8 January 2011. Modifications to the NLCD 2011 dataset included reducing the areal extent of the Great Salt Lake to reflect the lake state at that time as well as changing the characteristics of a number of land use classifications (e.g., urban and barren land) to more closely match albedo observations obtained during PCAPS. Snow cover obtained from North American Mesoscale (NAM) reanalysis was also modified to better match observations.

The resulting model simulation for the 1-8 January 2011 period was notably improved compared to an 'out-of-the-box' run for the same period relying on the default U.S. Geological Survey (USGS) and unmodified NAM reanalysis snow cover data. The most substantive improvements were observed within the Salt Lake and Cache Valleys, where modifications to the areal extent of the Great Salt Lake and improved snow cover

allowed for a more realistic simulation. The time of model initialization relative to the onset of the CAP was found to be a less critical factor than the improvements to land use and snow cover.

TABLE OF CONTENTS

LIST OF TABLES

LIST OF FIGURES

ACKNOWLEDGEMENTS

I would like to acknowledge my advisor, John Horel, for sharing his time and expertise with me as I pursued my master's degree. I would also like to thank Erik Crosman; his guidance and helpfulness were paramount in the successful completion of the thesis herein. To my committee members, John Lin and Sebastian Hoch, I want to say thanks for taking the time to read and sincerely respond to my research. Your comments and suggestions made me consider aspects of this topic I might not have otherwise. I would also like to recognize Nola Lucke, the glue that holds the Horel group together, who made traveling to conferences, such as the WRF New Users' Tutorial, easy and painless.

We thank C. David Whiteman for furthering the scientific understanding of cold pools that served as a basis for the questions presented in this thesis, as well as for leading the Persistent Cold-Air Pool Study (PCAPS), data from which are referenced heavily in this text. The comparison of the model simulations to PCAPS observations was made possible by the National Science Foundation project ATM-0938397.

I would like to acknowledge the support and funding provided by Utah Division of Air Quality for the purpose of this research. Finally, the Center for High Performance Computing at the University of Utah made the model simulations presented in this study possible through their allocation of computing time. Without those resources, a lot of this work could not have been accomplished in a timely manner.

CHAPTER 1

INTRODUCTION

During the winter months, midlatitude basins are often affected by multiday cold-air pools. The term cold-air pool (CAP) refers to cold air filling a bowl-like topographic feature. They most often occur and/or strengthen when cold air is trapped within a basin while the overlying air warms (Lareau et al. 2013). A number of meteorological factors affect the evolution of CAPs, including: cold fronts, which can deposit snow at the onset or help scour multiday events; warm air advection aloft within the predominant synoptic wind pattern prior to cold frontal passage; clouds present during the event as humidity within the boundary layer increases or higher clouds pass over the region; incoming solar insolation, as affected by the presence of clouds; surface radiative cooling, as affected by land and soil thermal properties and snow cover (Lareau et al. 2013). The vertical temperature structure associated with persistent CAPs is typically a combination of a (1) near-surface inversion associated with radiative nocturnal cooling and (2) an elevated temperature inversion associated with large-scale subsidence, downslope winds over the terrain, warm air advection aloft, and cloud top cooling. These diurnal near-surface cold pools (inversions) typically strengthen at night with radiative cooling and weaken or are completely mixed out during the afternoon, due to daytime heating expanding the boundary layer. In the afternoon, these mixed layers typically have strong capping inversions

remaining intact above them, which inhibits vertical mixing of the air within the valley to the free troposphere for many days, resulting in air stagnation and poor air quality as particulate pollution from residential, industrial, and automotive sources accumulate (Whiteman et al. 2014).

Multiday CAPs in Utah's Salt Lake Valley (SLV) are notorious for their poor air quality (Silcox et al. 2012; Lareau et al. 2013; Whiteman et al. 2014) and high concentrations of fine particulate matter ($PM_{2.5}$) are known to have adverse health effects on the population (Reitze 2014). Anthropogenic emissions from automobiles, industry, and home heating become trapped within the valley and the limited horizontal and vertical ventilation results in poor air quality. Snowstorms preceding the establishment of a CAP can provide the ingredients necessary later on (snow cover, low temperature, high humidity) that aid in the saturation of the boundary layer, which commonly results in dense fog and negative impacts on ground and air travel (Lareau et al. 2013).

The Persistent Cold-Air Pool Study (PCAPS), which took place in the SLV from December 2010 to February 2011, "addressed the need for modern observations capable of resolving the hierarchy of scales affecting persistent CAPs" (Lareau et al. 2013). The primary goal of PCAPs was to improve the meteorological understanding of the formation, maintenance, and decay of multiday CAPs. A number of studies have examined aspects of CAPs that occurred during the PCAPS period, including boundary-layer characteristics and pollutant concentrations (Silcox et al. 2012; Whiteman et al. 2014; Whiteman and Hoch 2014; Whiteman and Young 2015), synoptic interactions with CAPs (Lareau et al. 2013), and numerical weather prediction (Wei et al. 2013; Lu and Zhong 2014).

The evolution of CAPs is affected by the underlying surface state (Billings et al.

2006; Lareau et al. 2013). Common to most urbanized basins, the topography and land use characteristics within and surrounding the SLV are complex (Fig. 1.1). The underlying surface state has evolved over the past several decades—the SLV has rapidly become urbanized, while the nearby Great Salt Lake (GSL) level, and thus surface area, has decreased. The SLV slopes downward from south to north toward the GSL and is constrained by the Wasatch Mountains to the east, the Oquirrh Mountains to the west, and the lower Traverse Mountains to the south (Fig. 1.1). A number of flow patterns manifest in the SLV as a result of this topography, which can impact the evolution of CAPs, as well as the transport of pollutants within the valley. These flows include lake breezes (Crosman and Horel 2015), slope flows, gap flows (Pinto et al. 2006), and mountain wave terrain interactions (Lareau and Horel 2015).

Surface conditions during CAPs can change rapidly as snow is deposited beforehand from passing storms, metamorphosizes, and eventually may be removed. Neemann et al. (2015) simulated the effects of higher albedo associated with fresh snow cover in the Uinta Basin of eastern Utah on the atmospheric boundary layer. High albedo increases reflection of daytime solar radiation from the surface and thus, less energy is available near the surface to warm the atmosphere. This results in a lower sensible heat flux and lowering of surface air temperature, both of which are favorable for maintaining CAPs. The cooling effects of snow cover on the near-surface boundary layer combined with warming aloft associated with upper level ridging over the western United States maximizes the potential longevity and intensity of a CAP (Lareau et al. 2013).

The evolution and duration of CAPs are often poorly forecast by numerical weather prediction (NWP) (Billings et al. 2006; Baklanov et al. 2011). Errors in the vertical

temperature structure, cloud cover, and wind fields associated with inaccurate NWP of CAPs results in poor air quality modeling and forecasts (Reeves et al. 2011; Holtslag et al. 2013). Improving meteorological input for air quality and photochemical modeling is a critical research need (Christopher Pennell, Utah DAQ, personal communication). Potential deficiencies of operational and research models affecting their performance in simulating CAPs include misrepresentation of: (1) current static land use (e.g., recently urbanized vs. previously scrubland or agricultural); (2) dynamic land cover (e.g., incorrect specification of the amount or albedo of snow cover); or (3) initialization fields (e.g., poorly specified low-level stability in valleys and basins). These deficiencies ultimately affect the model through interactions with surface state characteristics, such as albedo, roughness length, heat capacity, etc., as well as through their influence on the surface energy budget. For example, increased snow cover would increase the albedo and reduce the roughness length of the associated area within the model, affecting the warming of the near surface atmosphere and the turbulent mixing and dispersion within it. This study investigates improving the land use, land cover, and snow cover during a persistent CAP episode in the urbanized SLV, Utah. Background and prior work related to identifying and resolving some of these deficiencies are now summarized.

Updated assessments of land cover and land use are a fundamental need for modeling studies sensitive to land-atmosphere interactions. While some long-term changes in land cover are a result of natural processes, human activity has an undeniable influence on any land-air interactions (Jin et al. 2013). Jin et al. (2013) describe the methods used to create the National Land Cover Database (NLCD) 2011 land use dataset, released for use with the most current Weather Research and Forecasting (WRF) model in April 2015. The

NLCD 2011 dataset builds upon the 2006 dataset by using change detection algorithms, which attempt to detect areas of spectral difference in Landsat imagery between 2006 and 2011, whether they be natural or anthropogenic in nature, and adjust the land surface accordingly.

Few studies have quantified the improvements that result from updated static land use in numerical simulations. Sertel et al. (2010) found that numerical simulations for the Marmara region of Turkey using more accurate land use data were more accurate than those relying on outdated land cover datasets. The U.S. Geological Survey (USGS) land use data are often used by default within the WRF Model and are derived from Advanced Very High Resolution Radiometer (AVHRR) satellite data retrieved in 1992 and 1993. Cheng et al. (2013) determined that the USGS land use data incorrectly classified most land use types evident in 2007 on the island of Taiwan. They found that another land use dataset available for use in WRF based on Moderate Resolution Imaging Spectroradiometer (MODIS) satellite products better represented most land use type distributions on the island, except in the island's heavily urbanized western region. A third land use dataset, obtained from 2007 Systeme Probatoire d'Observation de la Terre (SPOT) satellite imagery, was used as well. Based on separate model simulations using each of the three land use datasets, Cheng et al. (2013) found that improving land use classification resulted in improved model performance. Incorrect land use and land cover specification, arising mainly from the urbanization and deforestation underway in Taiwan, had a very noticeable impact on mesoscale land-sea breeze interactions and urban heat island effects.

As described by Cheng et al. (2013), these impacts arise from the variation between each dataset in terms of the heat capacity of the land surface, vegetative fraction, and

roughness length of the underlying surface, which influence the exchange of heat and momentum between the land and air. These variables affect the surface energy balance of the mesoscale features in different ways. If a model grid point is incorrectly classified as any nonurban category (i.e., cropland), it will have associated parameters that also incorrectly represent it. The urban heat island effect results from the characteristically low albedo and high thermal inertia, high roughness length, and low moisture availability of urban areas relative to surrounding, rural areas (Cheng et al. 2013). The low albedo of urban surface material allows for increased absorption of solar (shortwave) radiation, while the higher thermal inertia reduces the effect of radiative cooling. High roughness lengths are associated with weaker winds, which inhibits the turbulent exchange of heat within the boundary layer. All of these processes would not exist in an area incorrectly classified as 'cropland,' impacting the simulation of mesoscale processes such as the urban heat island, and in a similar way, land-sea breeze interactions (Cheng et al. 2013).

Due to the shallow nature of the boundary layers associated with CAPs, small perturbations in the surface state of the model can have significant impacts on their structure and evolution. Normally, daytime heating promotes instability and the expansion of the convective boundary layer, replacing the nocturnal surface-based inversion that form as a result of radiative cooling with a daytime mixed layer. However, in the presence of snow cover and its elevated albedo, afternoon destabilization of the boundary layer is less likely to occur as more solar radiation is reflected by the Earth's surface, as opposed to absorbed/reemitted. In the WRF model, the underlying surface has a specified albedo, based upon seasonably varying characteristics such as leaf area index, while snow has an albedo determined by its age (Chen et al. 2014). The effective albedo used by the Noah

land surface model within WRF is then calculated based on characteristics of the land surface (i.e., designated maximum albedo attainable by the land surface and height at which snow fully covers the land surface) and the snow covering it (i.e., depth and age). For example, the same layer of snow covering an urban area in WRF results in a lower effective albedo than if it covered barren land or shrub. Hence, snow albedo must be treated carefully over the diverse surfaces of northern Utah, which range from densely populated urban areas to playa, scrubland, barren land, and water. Outgoing solar radiation is computed as a fraction of the incoming solar radiation using the albedo derived in this fashion. Neemann et al. (2015) found that WRF model simulations of a CAP in Utah's Uinta Basin improved when: (1) the initialization fields of snow cover and snow water equivalent were manually adjusted to more closely resemble observations, and (2) variables that impact the interaction of snow and the land surface were also adjusted. However, the static and dynamic land use and land cover parameters appropriate for the Uinta Basin are simpler than those needed for the complex urban environment in the SLV.

Differences in the specification of the initial state, such as lead-time (model spin up time) or the source of initial and boundary condition data, may not have as large an impact as differences in the physics package or vertical mixing or eddy diffusivity parameters (Gallus and Bresch 2006; Possner et al 2014). However, Possner et al. (2014) found that large-scale subsidence was reduced in simulations with longer lead times for the Bay of Biscay region.

The major shortcomings of atmospheric models to simulate CAPs (or more broadly, stable boundary layer structures) presents a unique challenge. These include the over-estimation of wind speed, which will hasten the turbulent erosion of persistent CAPs

(Rakovec et al. 2002), a dependence on upper level features, such as ridges and troughs, which are highly influenced by initial and boundary conditions (Reeves and Stensrud 2009), and the complex interaction between forcings at the synoptic, meso, and microscale that result in these events (Baker et al. 2011).

The main objective of this study is to evaluate the impact of improving the land use and snow cover initialization in WRF simulations during CAPs. In order to reach this objective, the following questions are addressed on the basis of a case study of the 1-8 January 2011 CAP that occurred during PCAPS:

1) Does improved treatment of WRF model parameterizations of static land use and dynamic land cover and the corresponding changes in surface albedo and other surface properties affect the simulated temperature, wind, and cloud cover fields at both the surface and in the vertical?
2) Does improving the specification of the aforementioned fields in the model lead to closer correspondence of the model simulations to the conditions observed?
3) To what extent are the model simulations for this case sensitive to the timing of the initialization of the model, i.e., starting before or during the onset of the event?

As detailed in the next chapter, a modified version of the NLCD 2011 dataset will be implemented into the current WRF Version 3.7 build and used to simulate the 1-8 January 2011 CAP. Results follow in Chapter 3 with a summary and conclusions in Chapter 4.

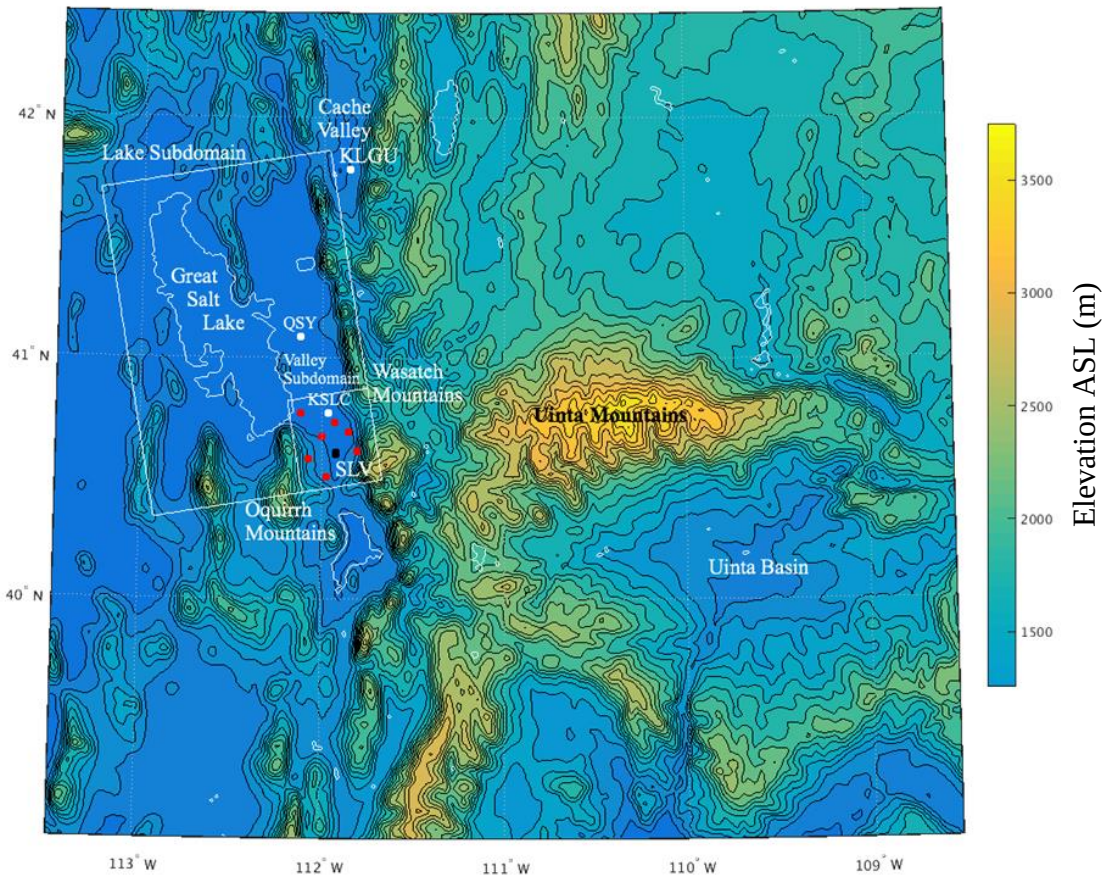

Figure 1.1. Terrain elevation in northern Utah and southwestern Wyoming shaded according to the scale on the right and contoured at an interval of 150 m. Rectangles enclose the Lake and Valley subdomains and colored dots denote observation locations discussed later.

CHAPTER 2

DATA AND METHODS

2.1 Observational Data

A wide array of observational data in the SLV was collected during PCAPS, particularly during the period of interest for this study, 1-8 January 2011 (Lareau et al. 2013). The location of a subset of PCAPS observations used in this study are shown in Fig. 1.1 and 2.1, including seven National Center for Atmospheric Research (NCAR) integrated surface observing system (ISFS) stations and two integrated sounding system (ISS) stations indicated by red and black dots, respectively, in both figures. The ISFS sensors included three-dimensional sonic anemometers, fast response temperature and humidity sensors, radiometers, and soil temperature probes. Five-minute averages of these data were used for the purpose of model validation in this study. Their locations were chosen to capture the geographical extent and varied land use of the SLV (Lareau et al. 2013). Further details on the land use type distributions associated with each of the 7 ISFS stations are given in Section 2.3.3.

Lareau and Horel (2015) merged a number of datasets including vertical profiles of wind and virtual temperature collected ISS sites (Fig. 2.1) and soundings launched during intensive observation periods to create interpolated time-height profiles of temperature, moisture, and wind representative of conditions in the central SLV. The time-height data

are available at an hourly resolution for the entirety of the PCAPS time period. These data help to evaluate how well the model simulated the temporal and vertical evolution of the CAP that occurred during 1-8 January, 2011.

In addition to the special data collected as part of the PCAPS field campaign, the MesoWest cooperative network (Horel et al. 2002) was used to gather surface weather observations from a variety of permanent stations throughout the SLV and the state of Utah. These observations are used in conjunction with the ISFS stations deployed strictly during PCAPS in order to perform surface validation of temperature and snow cover. Snow Telemetry (SNOTEL) snow depth data from mountainous stations located along the Wasatch front, along with Community Collaborative Rain, Hail, and Snow Network (CoCoRaHS) and National Weather Service (NWS) stations at lower elevations, are used to estimate snow depth as a function of elevation in the region.

2.2 Control Run WRF Model Setup

The simulations of the persistent CAPS that occurred from 1-8 January 2011 were conducted with the WRF model version 3.7. The control or 'base' simulation was initialized at 00 Z on 31 December 2010 and terminated at 00 Z on 9 January 2011. The initial and boundary conditions were obtained from the North American Model (NAM) operational analyses available from the NOAA National Operational Model Archive and Distribution System. A modified version of the NLCD 2011 land use dataset was used, along with modified snow depth and snow water equivalent fields, both adjusted based on available observations following Alcott et al. (2013) (as described in Section 2.3.1 and 2.3.2, respectively). The base model configuration consisted of three domains, as shown

in Fig. 2.2. The outermost domain (12 km horizontal resolution) encompassed the western U.S., while the innermost (1.33 km horizontal resolution) was situated to capture three subbasins in northern Utah: the SLV, the Cache Valley, and the Uinta Basin. A summary of the WRF model configuration is found in Table 2.1. Physics options used included the NOAH Land Surface Model, Mellor–Yamada–Janjic planetary boundary layer scheme, and Rapid Radiative Transfer Model (G) radiation. A modified version of the NLCD 2011 land use dataset was utilized.

2.3 Description of 1993 USGS and 2011 NLCD Land Use

Figures 2.3 and 2.4 highlight some of the differences in the three static land use datasets currently available for use in WRF version 3.7 discussed in this study, namely the USGS, and the NLCD 2006 and 2011 versions. (A MODIS static land use dataset circa 2000 is also available in WRF but will not be discussed in this study because it is less accurate in depicting the areal extent of the GSL and urban portion of the SLV.) Figure 2.3 shows the land use category of each grid point within the Lake subdomain (see Fig. 1.1). The areal extent of the GSL differs in each of the three unmodified land use datasets, with the NLCD 2011 having the largest areal extent. The percentage of water within the Lake subdomain for each unmodified land use scheme are: 24, 23, and 26 % for USGS, NLCD 2006, and NLCD 2011, respectively.

Figure 2.4 shows the land use category of each grid point within the Valley subdomain (Fig. 1.1). The urban expansion within the valley is primarily evident from the early 1990s (USGS land use) to that in 2011 (NLCD 2011). Only 15 % of the valley domain is classified as urban (urban and built up land) in the USGS dataset, whereas 41 % is

classified as urban (all 4 categories of urban considered, as shown in Table 2.2) in the NLCD 2011 dataset.

2.3.1 WRF NLCD 2011 Land Use Modifications

While the availability of the NLCD 2011 land use dataset improves the specification of urban areas in the SLV, the areal extent of the GSL is overdone (Fig. 2.3 c). Figure 2.5 shows the limited areal extent of the GSL in January 2011 relative to those specified by the land use classification available in WRF version 3.7 (Fig. 2.3 c). The NLCD change detection algorithm used to update the land use dataset from 2006 to 2011 used two pair of satellite images during the fall, specifically 2005/10/22 vs. 2011/10/23, and 2007/09/26 vs. 2011/08/20. The problem with this lies in the natural seasonal and inter-annual variations in land cover experienced in this area, including changes in the level of the GSL and snow covering Farmington Bay, the south-eastern section of the lake. These discrepancies affect the surface energy budget within the Salt Lake Basin as model grid points classified as water cannot be covered by snow and the albedo of water is much lower than that of snow covered barren land (or any other land cover classification).

The NLCD 2011 dataset was modified to more accurately portray the lower GSL level and areal extent during the winter of 2011 compared to that represented in the NLCD 2011 dataset. Figure 2.3d shows these changes, which are outlined as follows:

- Remove two rows of shore grid points of shallow GSL water and replace with land along northwest shore of lake.
- Remove unrealistic hook on west of lake.

- Remove detached body of water to northwest, which was frozen and covered in ice and snow.
- Remove unrealistic bay in southeast portion of the GSL (also covered in ice during IOP5, as seen in satellite imagery) by making it barren land, which can then be snow-covered in model.
- Trim southern portion of the GSL, since the surface appears to be snow and/or ice covered in satellite imagery.
- Reduced areal extent of seasonal marshland in northeastern portion of the lake.

The removed water grid points were replaced by barren land within the geo_em files created by the WRF preprocessing tool, geogrid.exe and all associated land surface properties (e.g., albedo, surface roughness) associated with barren land were applied to them. After modifications, the areal extent covered by water within the Lake subdomain is only 18 % (Table 2.2). Additional changes to the GSL state were made following Alcott et al. (2013):

- The saturation vapor pressure was decreased by 15% over the southern GSL and by 25% over the northern portions of the GSL to account for the water's salinity and allow for more realistic surface sensible heat flux and latent heat flux from the lake surface.
- The lake temperature was reduced from 1.2 ^{o}C (based on data available from the NAM initial conditions) to 0.5 ^{o}C as estimated from satellite following Grim et al. (2013).

2.3.2 Prescribing Initial WRF Snow Cover

This study defines the initial and boundary conditions from the NAM Reanalysis dataset. As will be shown later, the NAM analyses erroneously represented the spatial coverage of snow depth and snow water equivalent within the SLV at the onset of this event, extending an arm of high snow depth from the Wasatch Mountains to the east, into the central portion of the valley. Prior to the onset of the CAP, a winter storm deposited fresh snow with lower (higher) depths at low (high) elevations. Hence, the meteorological data files created by the WRF preprocessing system were modified to more closely follow the elevation dependence of the snowfall. Snow depth as a function of elevation was defined subjectively, as detailed in Fig. 2.6, following the approach of Alcott et al. (2013) and Neemann et al. (2015). Observations in the vicinity of the SLV from PCAPS, SNOTEL, CoCoRaHS, and NWS sites, as well as MODIS imagery, were used as a basis for formulating this function. The snow depth function was applied to the portion of northern Utah that was assumed to be impacted by this winter storm.

2.3.3 Modifications of Vegetation Parameter Table

The intended diversity of the siting of the ISFS locations is evident in Fig. 2.7, which outlines the land use type distribution surrounding each ISFS station within the NLCD 2011 dataset (see Fig. 2.1 for locations of each ISFS station within the SLV). ISFS 1 and the area surrounding it are primarily classified as ‘barren land,’ which has a characteristically high maximum albedo attainable by the model (MAXALB), low roughness length (Z0 in model or Z_o), and low height to which snow depth must reach in order to fully cover vegetation (SNUP). All grid points within the area surrounding ISFS 2

through 4 are classified as ‘urban,’ while the majority at ISFS 5 are also, with varying amounts of low, medium, and high intensity. More specifically, ISFS 2 was situated within the main downtown center of Salt Lake City, whereas ISFS 3 and 4 were in suburban areas in the east and west parts of the valley, respectively, and ISFS 5 is located in a residential area on the eastern slope of the valley, with nonurban grid points nearby. The remaining stations were situated in less densely populated areas within the valley. ISFS 6 represents an open, farmland-type area, and ISFS 7 a sparsely populated suburban community. The diversity in land use types at the 7 stations for which albedo observations are available during PCAPS presents the unique opportunity to evaluate model performance based on specific and identifiable land use classifications.

Neemann et al. (2015) discovered disparities between simulated WRF albedo and observations in Utah’s Uinta Basin resulting from two factors: 1) unrealistic SNUP, which WRF utilizes to parameterize albedo from snow cover and land use; and 2) reduced allowable values of MAXALB for fresh snow cover. Because of the effects these parameters can have on the simulation of persistent CAPs, the WRF vegetation parameter table (VEGPARM.TBL) was examined and the model specified albedos were compared to those observed.

Table 2.4 compares the observed albedo averaged from 1-8 January 2011 and MAXALB for the ISFS locations. While the albedo at ISFS 1 averaged 0.81 during this time period, the maximum albedo allowed for by barren land, prevalent in the Lake subdomain, is 0.75. This disparity is larger in the case of shrub/scrub, which has a maximum albedo of 0.60. To allow the model to potentially increase the albedo to the values observed, the MAXALB for each was raised to 80 (0.80). The SNUP of these land

use classifications was also modified such that less snow was required to cover the vegetation, allowing for a higher albedo to be possible, as well. For example, the SNUP over the playa surface that NLCD 2011 generally classifies as barren land was decreased to 0.01 m, i.e., 0.01 m of snow water equivalent (roughly 10 cm of snow) is more than enough snow to cover the smooth playa surface that surrounds the GSL. All modifications to the MAXALB and SNUP for other land use classifications represented by each station are summarized in Table 2.4, as well.

2.4 Numerical Sensitivity Studies

In order to examine the sensitivity of CAP simulations to land use, snow cover, and initialization time, four model runs will be described here for the 1-8 January 2011 period. They will be referred to as follows:

1. BASE: Using NLCD 2011 modified land use and modified snow cover, initialized on 31 December 2010.
2. USGS: Using USGS land use and NAM Reanalysis snow cover, initialized on 31 December 2010. (This land use choice would be the default for WRF version 3.7. The NAM reanalysis snow fields are unmodified.)
3. DEC30: Using NLCD 2011 modified land use and modified snow cover, initialized on 30 December 2010.
4. JAN01: Using NLCD 2011 modified land use and modified snow cover, initialized on 1 January 2011.

The BASE and USGS simulations will be compared in order to determine the sensitivity to changes to the default static land use and the dynamic land cover including

snow cover and albedo. The physical differences in GSL areal extent and snow depth between these two simulations are summarized in Fig. 2.8. Specifically, the differences between BASE and USGS can be classified as pertaining to static fields, initialization, and dynamic land use in the following manner:

- Static Land Use: 1) Modified areal extent of the lake (Fig. 2.8a). 2) Differences in land use classification between the two land use datasets (Fig. 2.3a versus Fig. 2.3d and Fig. 2.4a versus Fig. 2.4d).
- Snow Initialization Fields: 1) Snow cover spatial extent, depth, and snow water equivalent specifications (Figures 2.6 and 2.8b).
- Dynamic Land Use: 1) Modifications to albedo parameterization table (Table 2.4), which impact the interactions between snow properties and static land use in the NOAH land surface model.

Considering the dynamic interplay between each of these changes, the sensitivity of the model to each specific modification will not be presented here. Rather, an overall influence of all these changes, which attempt to more realistically simulate the surface state, will be discussed in Chapter 3.

The BASE run will then be compared to the DEC30 and JAN01 simulations, which will provide a basis for determining the effect of the initialization time on modeling the 1-8 January 2011 period. The only difference between these runs will be the date and time at which they are initialized, so that the effect of differences in the above surface initialization fields, i.e., the vertical stability and wind and moisture profiles on the simulations, can be ascertained.

Table 2.1. Summary of WRF setup and parameterizations.

Parameter	**Chosen Setup**	**Reference**
Initial/Boundary Conditions	NAM analysis	
Vertical Levels	41 ETA levels	
Domains	3 one-way nests	
Resolution	12 km, 4 km, 1.33 km	
Time Step	45 s, 15 s, 5 s	
Microphysics	Thompson	Thompson et al. 2008
Planetary Boundary Layer	Mellor-Yamada-Janjic (MYJ)	Janjic 1994
Land Surface	Noah	Chen and Dudhia 2011
Radiation (Short and Long Wave)	RRTMG	Iacono et al. 2008
Surface Layer	Eta Similarity	
Cumulus	Kain-Fritsch (12 km dom)	Kain 2004

Table 2.2. Summary of urban classification percentage in USGS and NLCD 2011 for the valley subdomain.

	Urban/Built-Up Land	Dev. Open Space	Dev. Low Intensity	Dev. Med. Intensity	Dev. High Intensity	Total Urban
USGS	0.15	N/A	N/A	N/A	N/A	0.15
NLCD 2006	N/A	0.03	0.21	0.08	0.06	0.38
NLCD 2011	N/A	0.02	0.19	0.17	0.03	0.41

Table 2.3. Summary of changes made to water and barren land classification in NLCD 2011 as compared to unmodified NLCD 2011 and USGS datasets with the lake subdomain.

	Water	**Barren Land**
USGS	0.24	0.10
NLCD 2011	0.26	0.12
NLCD 2011 Mods	0.18	0.20

Table 2.4. Summary of changes made to the vegetation parameter table.

	Model Land Use Classification	Station Average	SNUP (m of SWE)	MAXALB (%)	SNUP Adjusted	MAXALB Adjusted
ISFS 1	Barren Land	0.81	0.03	75	0.01	80
	Shrub/Scrub		0.03	60	0.02	80
ISFS 2	Dev High Intensity	0.74	0.04	46	0.04	70
ISFS 3	Dev Med Intensity	0.80	0.04	46	0.04	75
ISFS 4	Dev Low Intensity	0.77	0.04	46	0.04	75
ISFS 5	Dev Low Intensity	0.78	0.04	46	0.04	75
ISFS 6	Pasture/Hay	0.72	0.04	66	0.04	70
ISFS 7	Cultivated Crops	0.78	0.04	66	0.02	75

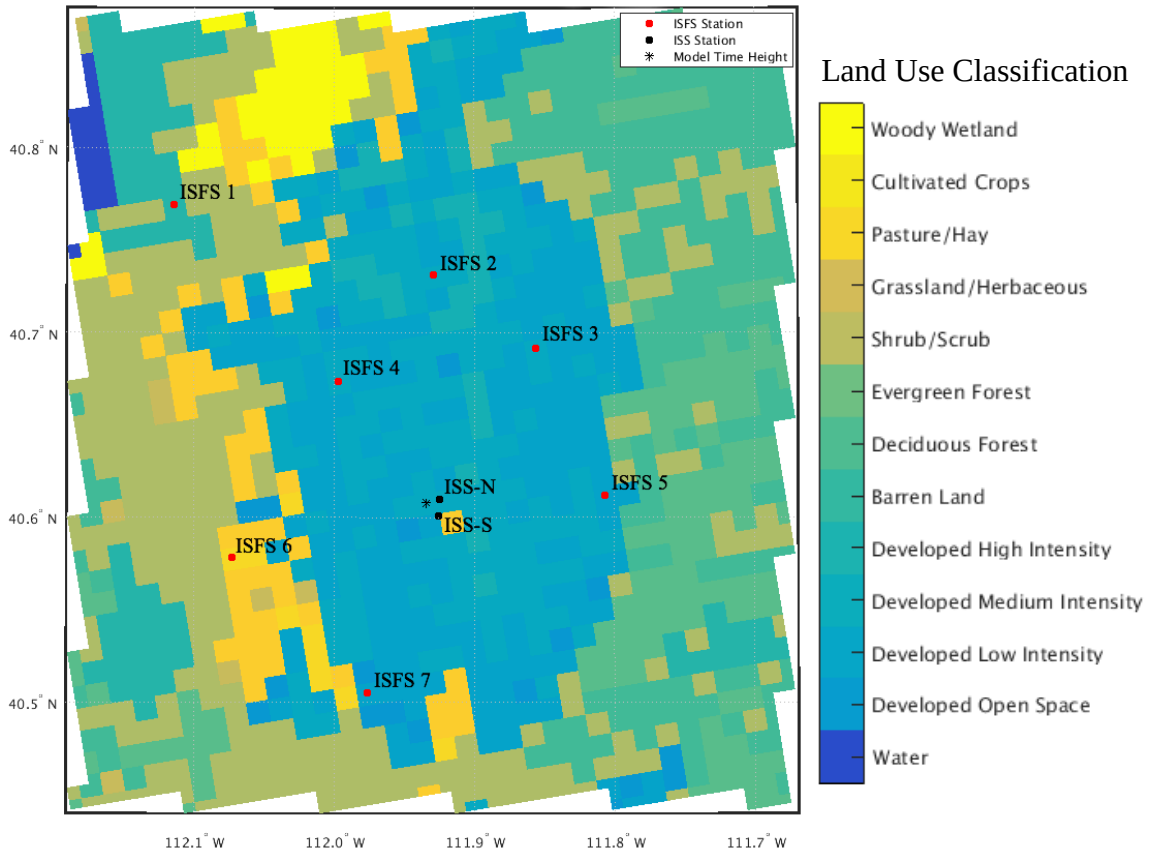

Figure 2.1. ISFS (red dots) and ISS (black dots) station locations deployed during the PCAPS field campaign of the 2010-2011 winter period. Station locations are plotted over the land use type distribution according to the color legend within the Valley subdomain indicated in Fig. 1.1. The grid point closest to the two ISS locations where time heights within the SLV are later plotted is indicated by the black star.

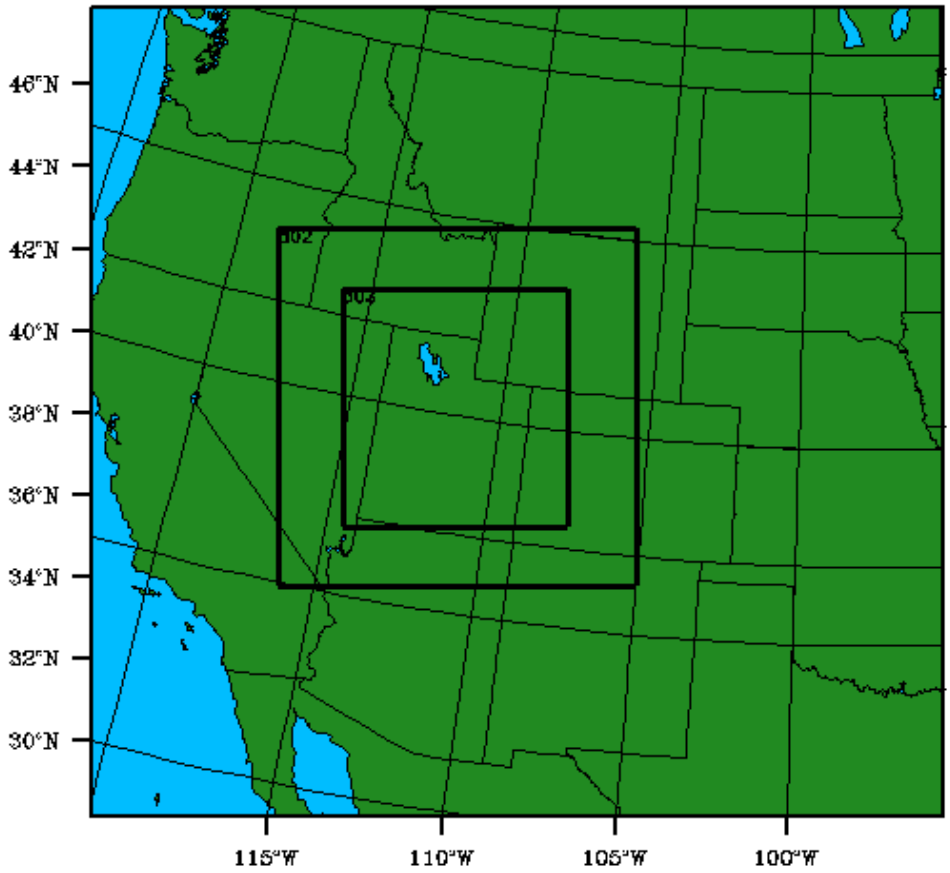

Figure 2.2. Nested WRF domains with grid spacing of 12, 4, and 1.33 km.

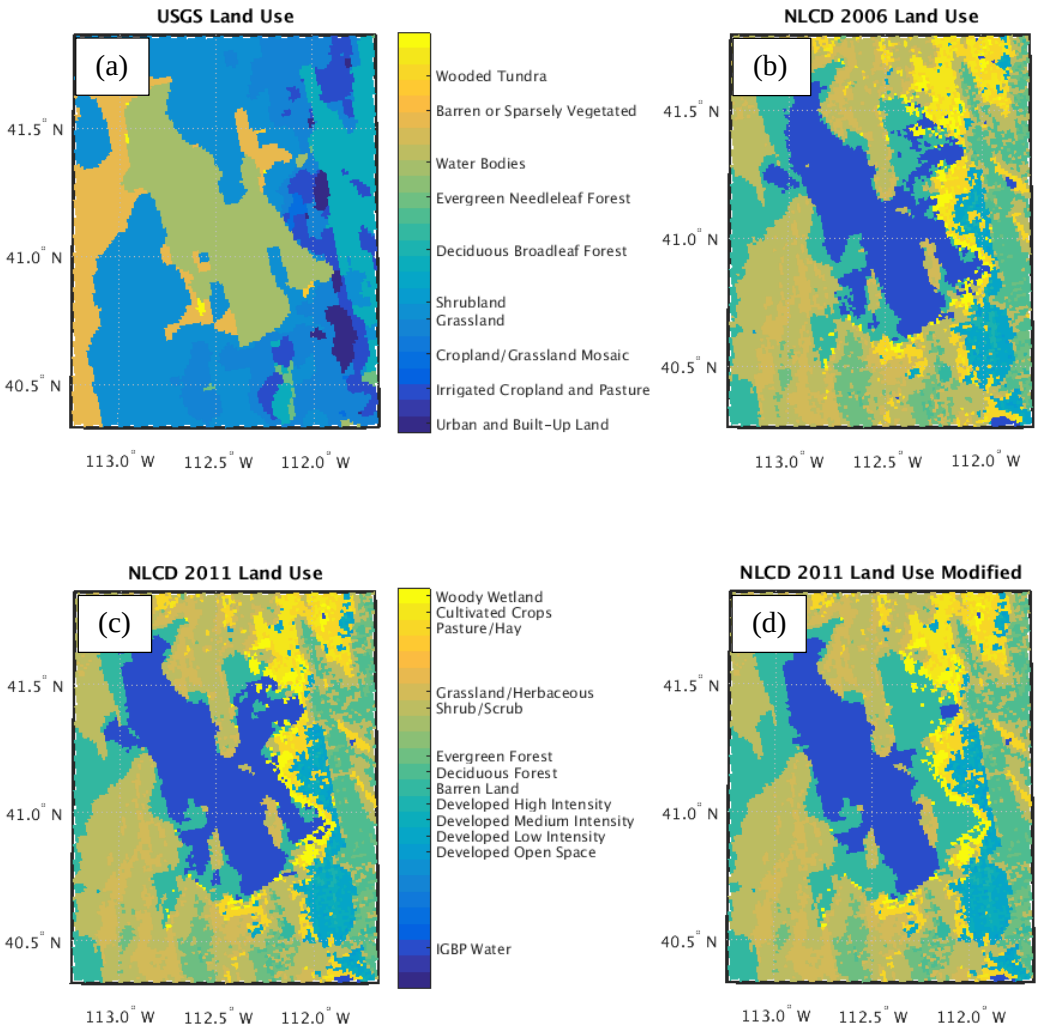

Figure 2.3. Land use classification within the Lake subdomain at 1.33 km resolution, corresponding to (a) USGS, (b) NLCD 2006, (c) NLCD 2011, and (d) modified NLCD 2011 (d). USGS and NLCD land use datasets utilize different classifications schemes, as shown in color legend.

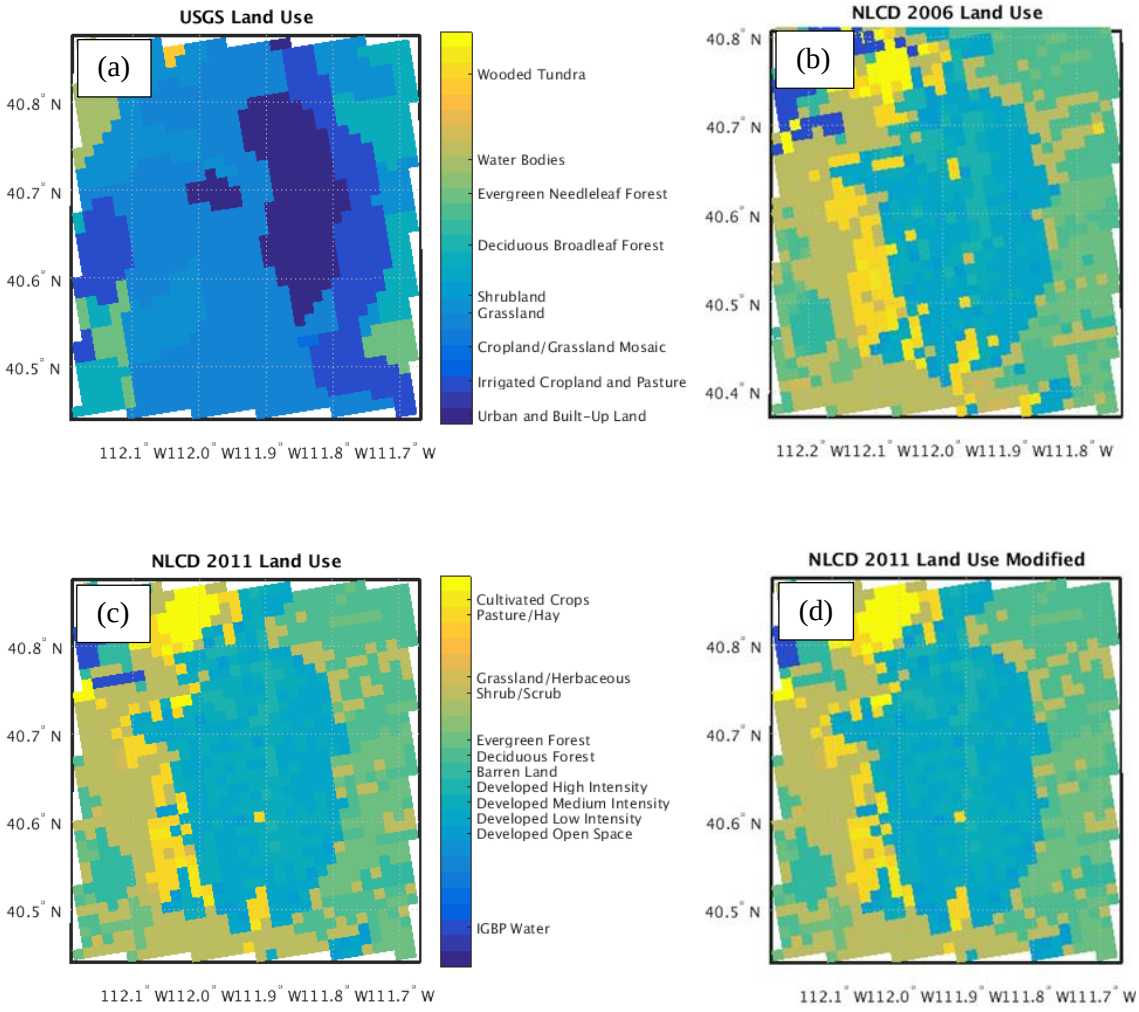

Figure 2.4. Land use classification within the Valley subdomain at 1.33 km resolution, corresponding to (a) USGS, (b) NLCD 2006, (c) NLCD 2011, and (d) modified NLCD 2011. USGS and NLCD land use datasets utilize different classifications schemes, as shown in color legend.

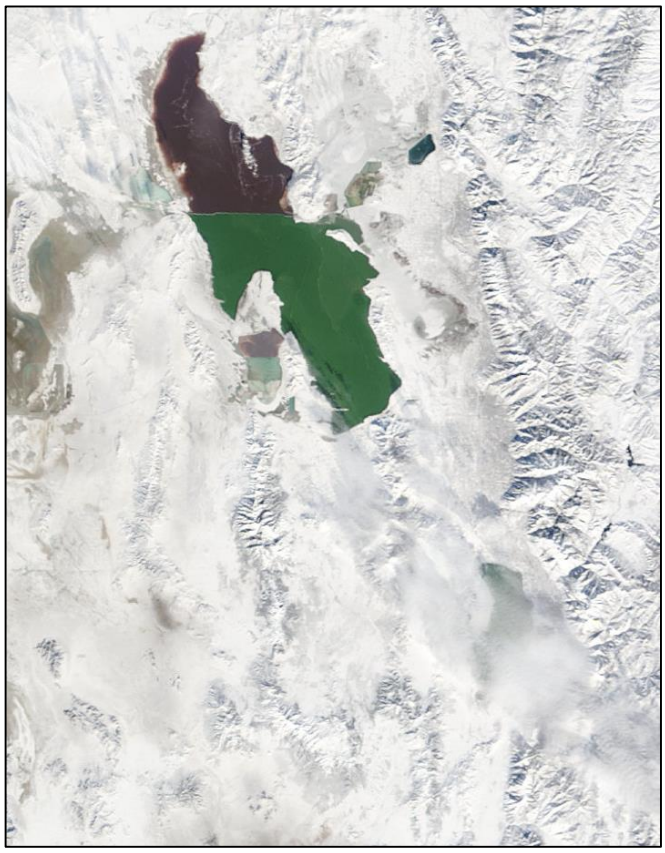

Figure 2.5. MODIS satellite imagery from the Terra platform on 1 January 2011 centered over the GSL and SLV.

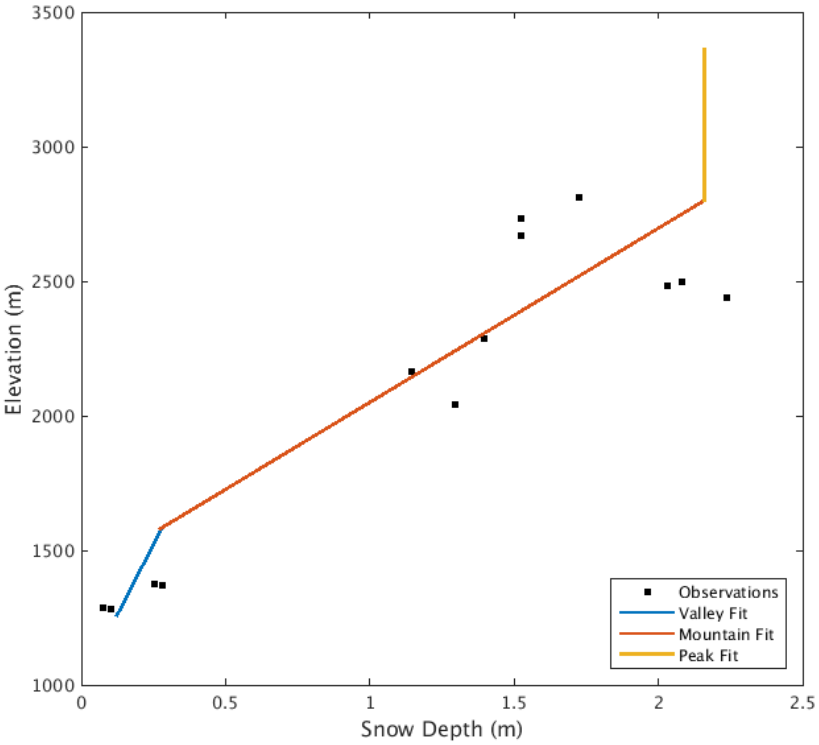

Figure 2.6. Idealized snow depth fit for valley (red), mountain (yellow), and peak (purple) elevations. Observations are represented by blue dots.

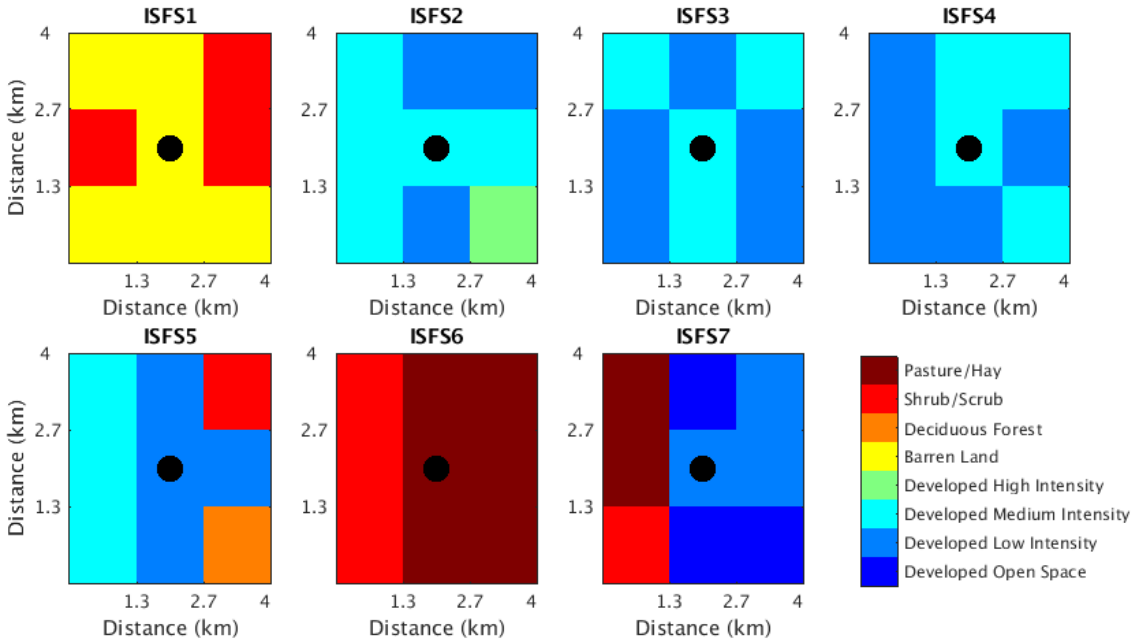

Figure 2.7. Three by three grid point display (16 km^2 area) of land use type encompassing each ISFS location indicated in Fig. 2.1. Black dots correspond to the station locations indicated by the red dots in Fig. 2.1.

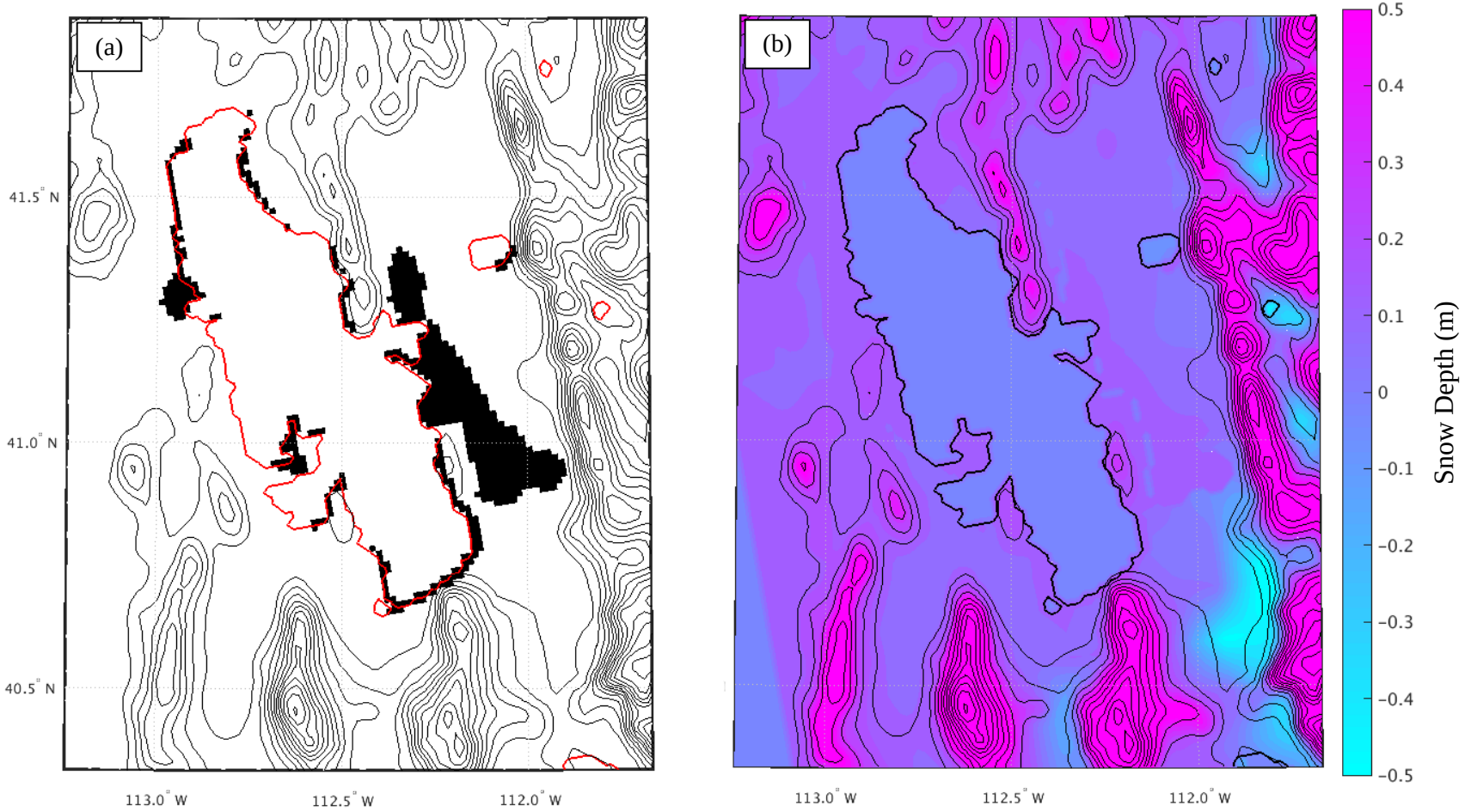

Figure 2.8. Elevation contoured as solid black lines at an interval of 150 m. (a) Grid points treated as water by USGS and not treated as such in BASE (black). (b) Difference in snow depth (m) (BASE – USGS) at first model hour.

CHAPTER 3

RESULTS

3.1 Overview

In this chapter, we discuss the sensitivity of modeled CAP characteristics (e.g., vertical structure, winds, temperature) to the specification of surface land use and initialization of the surface state. We also analyze the sensitivity of the simulations to variations in the initialization time. Because the surface land use and surface state remain constant between the various initialization time simulations, these simulations give insight into the sensitivity of CAP simulation evolution to the initial prescribed atmospheric state. The applied changes to the GSL surface area and initial snow cover depth between the UGSG and BASE simulations are illustrated graphically in Fig. 2.8. As shown in Fig. 2.8a and Table 2.3, the areal extent of the lake is decreased in BASE compared to USGS whereas differences in snow cover are more spatially variable (Fig. 2.8b). Deeper, more uniform snow depths now cover the lower elevation desert regions in BASE, particularly to the west and north of the GSL. However, the snow modifications discussed in Chapter 2 resulted in a localized decrease in snow depth within the eastern half of the SLV (lower right corner of Fig. 2.8b). The resulting spatial distribution of snow in BASE is judged to be more in line with that evident from satellite images (Fig. 2.5) and the snow depth and SWE in BASE agrees better than USGS with the available observations (Fig. 2.6).

This chapter is constructed in the following manner: First, an overview of the observed meteorological conditions during 1–8 January 2011 in the GSL Basin are presented in Section 3.2. The impact of the modifications applied to the BASE simulation compared to the USGS simulation (as discussed in Chapter 2) including changing the GSL's areal extent and snow cover over the GSL Basin (Fig. 2.8) are analyzed in Sections 3.3 and 3.4. In Section 3.3, we analyze several regions most impacted by changes in the specified snow cover and GSL areal extent. In Section 3.4, we focus on the impact of changes in urbanization, dynamic land use and albedo parameters (MAXALB and SNUP), and snow cover on CAP evolution in the SLV and use the PCAPS observations to characterize model improvements and weaknesses. Finally, results from two additional model simulations varying the initialization time to 30 December 2010 (DEC30) and 1 January 2011 (JAN01) are discussed in Section 3.5.

3.2 Overview of the 1-8 January 2011 CAP

The passage of an upper level trough across the western United States from 30 December 2011 to 1 January 2011 resulted in very cold air aloft (700 mb temperatures as low as -23.5 ^{o}C) and widespread fresh snowfall (e.g., roughly 5 cm at the Salt Lake International Airport, KSLC, in Fig. 1.1). In the wake of this upper level trough, an upper level ridge developed over the western U.S. from 1-9 January (Fig. 3.1), interrupted only by the passage of a weak upper level shortwave trough from 4-5 January. During this period, 700 mb temperatures increased to as high as 0 ^{o}C and remained above -10 ^{o}C, while surface temperatures remained consistently lower, resulting in a capping inversion that persisted for the duration of the CAP. The time-height evolution of potential temperature

and relative humidity shown in Fig. 3.2 for the central SLV is derived from data developed by Lareau and Horel (2015). On 1 January, a strong stable layer sets up overnight immediately above the surface. Later that day into the next, a capping inversion (i.e., the layer between 280 – 285 K in Fig. 3.2a) descends into the SLV. Daytime heating destroys the shallow nocturnal surface inversions on the 1st and 2nd. From 3-4 January, the stability of the nocturnal stable layer weakens, while the capping inversion remains in place, until the upper level disturbance impacts the region from 4-5 January. Colder air advects in during this event (see heightening of 285 K adiabat), but was not strong enough to fully erode the stable air mass below 1800m. The passage of the weak shortwave disturbance aloft on 3-4 January also increased the relative humidity aloft and eventually contributed to moistening of the boundary layer (Fig. 3.2b). After this event, the stability of the nocturnal boundary layer once again increased, then progressively weakened each day until the CAP reached an end later on 9 January (see 295 K adiabat lifting at the end of the time period in Fig. 3.2a). Near-surface relative humidity also increased during the last few days of IOP 5, as fog began to develop within the cold surface layer. This CAP exhibited the most intense potential temperature deficit between the surface and mountaintop level and had the most significant accumulation of near-surface pollutants observed during PCAPS (Lareau et al. 2013). These and other data collected during PCAPS will be used in this study to help validate the following numerical results.

3.3 Sensitivity to Great Salt Lake Areal Extent and Snow Cover

In order to examine the model's sensitivity during this case to modifications in the areal extent of the GSL, land use and snow cover, time series, and model run averages of

variables such as temperature, potential temperature, albedo, and cloud water mixing ratio from each run are compared. During winter, the elevation of the GSL is near its annual low. The shallow, low salinity areas often become covered in ice and snow, which is not captured by the NLCD 2011 land use dataset or the WRF model.

Figure 3.3 shows the BASE minus USGS difference in average albedo for the period 1-8 January 2011 within the Lake subdomain. Dark blue (red) colors denote areas where BASE has a lower (higher) albedo than USGS on average. The differences in albedo between BASE and USGS simulations shown in Fig. 3.3 result from the cumulative effects of 1) changes in snow depth, 2) changes in snow spatial extent, 3) changes in land use type (e.g., lake becomes snow-covered land), 4) changes in the vegetation parameter of maximum allowed albedo (MAXALB), and 5) changes in the vegetation parameter of the amount of snow required to cover the ground (SNUP). By far the most dominant effect on the observed differences evident in Fig. 3.3 corresponds to the adjustments made to the areal extent of the lake shown in Fig. 2.8. In the southeast section (Farmington Bay) where water was replaced by a shallow layer of snow cover, the albedo in BASE is much higher. In some areas, the average albedo increased by as much as 0.5. The next most pronounced factor impacting the differences in albedo between the two simulations is the increase in snow coverage and depth in the deserts surrounding the GSL. The albedo is generally increased in BASE within the lake subdomain (yellow, orange, and red shading), and areas where snow cover increased in BASE (Fig. 2.8b) tend to correspond with areas of increased albedo. An area of slightly decreased albedo in BASE (teal shading) within the eastern bench of the SLV coincides with an area of decreased snow depth in BASE (see Fig. 2.8b). Snow depth also increased in the Cache Valley, a region where albedo is increased in

BASE, as well (Fig. 3.3). As will be discussed in Section 3.4, some of the modest albedo increases between the BASE and USGS simulations in both the SLV and over the desert surfaces resulted from changes in the allowable MAXALB and SNUP parameter table in the urban and scrubland environments.

Figures 3.4 (3.5) show the difference in the average 2-m temperature (cloud water mixing ratio in first 10 model levels, roughly surface to 200 m AGL) between BASE and USGS. The average differences are calculated separately for day and night hours (1800 – 0000 UTC and 0600 – 1200 UTC) to highlight areas of peak warming and cooling, respectively. Dark blue (red) colors denote areas were the BASE average is less (greater) than the USGS average. While the 2-m temperature difference between BASE and USGS is more pronounced at night (Fig. 3.4b), the areas to the east and west of the lake that were modified show widespread differences of greater than 2 ^{o}C in magnitude during both day and night. The large nighttime differences (> 4 ^{o}C) likely result from the effects of limited sensible heat fluxes in BASE, now that areas surrounding the lake are comprised of snow covered land, as opposed to water or open (not snow covered) land surrounding the lake. In contrast, in the USGS simulation the higher heat capacity (and thus thermal inertia) of the GSL and its higher surface temperatures could offset the nighttime cooling in those areas surrounding the lake, keeping temperatures higher. By allowing surfaces that are known to be snow covered (based on satellite imagery and observation) the opportunity to be so, their albedo increased and the ability of the surface to absorb solar radiation and warm the near surface atmosphere through sensible heat flux decreased.

The differences in lake size and snow cover also correspond to differences in low level moisture and cloud cover. Along the eastern and western portions of the lake at night,

as well as during the day to the west, cloud water mixing ratio within the first ten model levels is higher in BASE compared to USGS (Fig. 3.5), which also corresponds to areas in which temperature was lower in BASE. These differences extend beyond where the lake boundary is modified, into areas where snow cover increased and land use changed between the two simulations. This increase in low-level cloud water mixing ratio, more pronounced at night, is likely an indication of the formation of radiation fog within the CAP. This process is aided by enhanced radiative cooling caused snow's high emissivity. Small decreases in cloud water mixing ratio in the BASE simulation compared to the USGS simulation along the mountain slopes may correspond to a lowering of the inversion and vertical restriction of the shallow saturated layer (Fig. 3.5).

Specifying snow where water is erroneously assumed can also impact the model's ability to capture the diurnal cycle in temperature. As shown in Fig. 3.6a, time series of BASE temperature compare relatively well to that observed at the Syracuse, UT, DAQ site, which is situated on the central eastern shore of the GSL when the lake level is at its maximum (QSY, see Fig. 1.1). BASE (blue) was able to capture the diurnal temperature cycle present within the CAP. While BASE often simulated nighttime minimum temperatures higher than observed, daytime maxima were simulated relatively well, although a slight lag is noticeable between the two time series. On the other hand, USGS was unable to capture the daily variations in temperature at Syracuse, remaining warmer than the observations (black) for the majority of the run and showed little distinction between day and night. BASE classifies the location of the Syracuse station as 'barren land', on the outskirts of 'woody wetland' and 'pasture/hay,' whereas USGS classifies the same grid point as part of the GSL. The difference in the thermal properties of snow

covered barren land and water can obviously impact diurnal variations in temperature. For example, the presence of snow covered land can reduce daytime heating and enhance nighttime cooling. On the other hand, the presence of water and its low albedo can allow solar radiation to be absorbed during the day and its high heat capacity aids in longwave radiation being emitted throughout the night, dampening diurnal fluctuations in temperature. In the Cache Valley (see Fig. 1.1), where snow depth increased and vegetation parameter albedo variables SNUP and MAXALB were corrected, nighttime minimum and daytime maximum temperatures decreased in BASE relative to USGS, resulting in a simulated temperature trace in BASE much closer to that observed (Fig. 3.7a), more so during the night.

Changes in the land use specification and snow cover also impact the vertical structure of the CAP. Figure 3.8 shows model time-height diagrams of temperature and cloud water mixing ratio located at Syracuse. While there are no boundary layer observations to compare these model results to, simply comparing BASE to USGS reveals that the physical changes made to the model influenced the simulation of the CAP. The CAP modeled in BASE (Fig. 3.8b) begins on 01 January and strengthens (or becomes more shallow) until the upper level system passes on 04 January. Then the CAP once again strengthens until its end on 09 January. The descending subsidence inversion present in Fig. 3.2a was simulated by both BASE and USGS; however, the diurnal surface inversions below 300 m AGL are much stronger in BASE. The presence of the underlying water surface at this location in USGS aids in producing higher surface temperatures than those of BASE, and the USGS run never develops the shallow nocturnal inversions present at this location during this event.

Near-surface (lowest 100 m) flow during CAPs is typically weak, but responds to the net horizontal and vertical variations in temperature and cloud cover. Figures 3.9 (3.10) show the average zonal (meridional) wind component over the period of 1-8 January 2011 for both BASE (panel a) and USGS (panel b). These averages computed over multiple diurnal cycles tend to reflect residual differences between down valley/land breezes at night and up valley/lake breezes during the day. The zonal (meridional) component will tend to highlight these residual differences on the western and eastern (southern and northern) peripheries of the lake. For example, the BASE zonal wind average has a stronger easterly nocturnal wind on the eastern shore since there is a land/water contrast there that is largely absent in the USGS due to the broader extent of its lake. On the southern end of the lake extending into the SLV and Tooele Valley to its west, southerly down valley/land breezes (deep red shading to southeast in Fig. 3.10 a) are weaker in BASE (Fig. 3.10b). In USGS, these down valley/land breezes are in part forced by the warm lake to the north and the cold, snow covered valleys to the south. In BASE, the SLV has less snow pack and the southeaster quadrant of the GSL is snow covered, creating less of a thermal contrast. The southerly land breeze flow present in USGS averages upwards of 3 m/s east of the elevated terrain in the southcentral region of the GSL. In BASE, the southerly winds in this area remain around 1 m/s and weaken considerably near and south of Syracuse. The land breeze in BASE was enhanced as compared to USGS within areas around the main body of the GSL where snow cover increased between runs. Thermally-driven valley flows are also much stronger in USGS, as seen when comparing magnitudes of the average meridional wind in Fig. 3.10 in the southern SLV. As has been observed in other modeling studies (e.g., Ahmadov et al. 2015, Neemann et al. 2015) the surface wind speeds in WRF

simulations of CAPs are generally higher than those observed. However, comparisons between PCAPS surface observations show that the BASE wind fields, particularly at night, agree better with observations than the USGS, likely because of more realistic surface forcing and horizontal temperature contrasts in the BASE configuration.

3.4 Sensitivity to Land Use and Snow Cover in the Salt Lake Valley

As described in Chapter 2, the NLCD 2011 land use classification used for the BASE simulation reflects a more urbanized environment than the USGS. In addition, modifications were made to WRF parameters in the BASE simulation (such as the maximum albedo, MAXALB, and the degree to which vegetation is covered by snow, SNUP, parameters, see Table 2.4) to more accurately represent how snow is handled as a function of the various NLCD 2011 land use categories. Figure 3.11 illustrates how observations of albedo during the day vary among the seven ISFS sites. Generally, the observed albedo remains above 0.70 when the snow is fresh (early during this period) and lowers to 0.65 and above later, due to snow metamorphosis (or aging) according to the land surface model. If the default values of MAXALB and SNUP are used for the USGS land use classifications (Fig. 3.11a), the albedo at the seven locations remains below 0.65 throughout the period and is as low as 0.50 at some sites. After all of the changes are made (Fig. 3.11b), the modeled albedo is higher and more uniform among the seven sites, yet still remains lower than that typically observed. Hence, the modifications made to the vegetation parameter table are conservative ones.

We now return to earlier figures focusing on the differences in the simulations within the SLV. In terms of surface temperature, BASE is warmer than USGS in much of

the SLV for the duration of the model run, during both day and night (positive differences in Fig. 3.4). Higher 2 m temperatures were simulated in the eastern half of the SLV in BASE, an area where snow depth was lower (Fig. 2.8b) and changes to land use included increasing the urban extent of the valley by over half (Table 2.2). However, areas in the western portions of the SLV and near the GSL observed lower 2 m temperatures resulting from the combined land use and land cover changes. Correspondingly, the low-level cloud water is also higher in the SLV in BASE (Fig. 3.5).

The time series of observed and simulated temperature in Fig. 3.12 at the seven ISFS sites help to evaluate the impacts of the land use and snow cover differences on the USGS and BASE model performance. Overall, the BASE model temperature time series trend towards the observations more closely than the USGS model temperatures. For example, at the downtown urban site (ISFS2), USGS temperatures (red) remain lower than BASE temperatures (blue), especially during the night. BASE temperatures tend to more closely follow observations than USGS particularly during the period from 4-7 January. Since ISFS 2, 3, and 5 fall within urban and suburban areas that have been built out for decades, any discrepancies between USGS and BASE likely result from the treatment of snow cover (specified snow depth, and SNUP and MAXALB variables). On the other hand, ISFS 4 and 7 are located in areas of the Valley that have undergone more recent development, so the differences in model performance in those areas likely are influenced by both sets of changes. The ISFS 1 site was selected to be representative of the playa regions surrounding the GSL, which is generally sparsely vegetated by scrub. It is classified as barren land by BASE and shrub/scrub by USGS. Both models fail to simulate the extremely low temperatures at night and overdo the temperatures during the day.

The physical changes imposed upon the BASE simulation – e.g., altering the areal extent of the GSL, adjusting the snow depth to better match that observed, and modifying albedo parameters such as MAXALB and SNUP – all have a complex, spatially and temporally varying effect on the modeled surface energy balance. The net shortwave radiation is modulated by the surface albedo, which varies as a function of snow depth, snow age, land use type, and the depth of vegetation. The net longwave radiation is even more complex, and is affected by a number of factors, including clouds, snow cover, and the thermal properties of the underlying land surface. The surface sensible heat flux (Fig. 3.13) is a useful proxy for gaining some understanding of how the surface energy balance impacts the exchange of sensible heat at the land surface and consequently the low-level temperature structure in the atmospheric boundary-layer during the CAP.

For example, at night, BASE has a lower surface heat flux than USGS over the portions of the GSL that were removed (dark blue in Fig. 3.13b). This is influenced by the changes made to the land surface (water in USGS and snow covered, barren land in BASE). Snow covered land is unable to absorb as much solar radiation during the daytime, and snow's high emissivity enhances nighttime radiative cooling. On the other hand, water's low albedo and high thermal inertia (heat capacity) increases the surface heat flux in USGS. Other areas where similar effects are noticeable are the Salt Lake and Cache Valleys. In the SLV, where the predominant land use classification became urban and snow depth decreased in BASE, the surface heat flux increased (oranges and reds in Fig. 3.13 a and b). Flow intensity and advection of warmer/colder air also has an influence on the surface heat flux in the SLV, by affecting the turbulent exchange of heat within the boundary layer and near surface temperature gradient. In the Cache Valley, where the only difference between

model runs is static land use and snow cover, there was a decrease in surface heat flux during the day in BASE (Fig. 3.13a). The increase in snow cover in this simulation reduced the absorption of shortwave and emission of longwave radiation during the day.

Figure 3.14 provides insight into the vertical structure and evolution of the CAP within the SLV modeled in BASE and USGS compared to that observed (Fig. 3.2). The USGS simulation exhibits much stronger surface-based inversions every night compared to those observed (Fig. 3.14a). This likely results from the excessive snow cover and resulting too low surface air temperatures in that model simulation. Comparing the potential temperature from BASE (Fig. 3.14c) to observations, BASE and USGS captured the evolution of the CAP relatively well. The capping inversion descended into the valley during the first two days, the upper level system moved through from 4-5 January and heightened the capping inversion, and finally the surface layer weakened during the last few days as the CAP began to erode late on 8 January. The presence of cloud water associated with the weak trough passage and stratus late in the period in the BASE simulation (Fig. 3.14d) has some similarity to that observed both in terms of the relative humidity time-height section as well as observations made of cloud cover during PCAPS.

Land use and snow cover affect flows at the surface through their influence on surface fluxes and roughness length. Fig. 3.9a shows strong, nocturnal downslope flows (positive zonal wind) along the western slopes of the SLV in USGS. The same flows in BASE (Fig. 3.10b) are weaker, and do not extend as far east, into the valley (~2 m/s average in USGS, as opposed to ~1 m/s in BASE). In this western part of the valley, USGS classified the land use type as shrubland and grassland, whereas it is mostly urban in BASE (Fig. 2.4). Shrubland and grassland have maximum roughness lengths of 0.05 and 0.12,

whereas all of BASE's urban classifications have maximum roughness lengths greater than 0.5 (up to 2.0 for developed high intensity). USGS also had a deep, unrealistic snow pack in place at the beginning of the simulation, which was replaced in BASE by a more realistic, terrain following snow pack within the valley. Similarly, Fig. 3.10a shows a 2-3 m /s nocturnal drainage flow extending through the SLV and across Farmington Bay in USGS. When the warm water in the Bay in USGS is replaced by snow in BASE, the strength of the temperature gradient between the Bay and the SLV is decreased, and the lake breeze flow significantly weakens in BASE.

These examples illustrate just a few of the many factors that played a role in the differences in wind speeds observed between the two model simulations, and provide a physical explanation for the stronger, farther-reaching downslope and drainage flows simulated by USGS, on average. The physical differences between BASE and USGS also affect flows above the surface (Fig. 3.15). The ISS site deployed during PCAPS was centrally located within the valley in an urban area, where the disparity between USGS shrubland and BASE urban classifications existed and deeper snowpack existed in USGS. Figure 3.15 shows stronger winds from a slightly elevated southerly jet reached closer to the surface in USGS, as opposed to BASE, during the time periods when it was present, such as 1-2 and 5 January, 2011. Both the USGS and BASE vertical profiles of meridional winds at ISS have stronger near surface winds compared to observation (3.15 a). Higher wind speeds impact the simulations by increasing the turbulent exchange of heat within the boundary layer. This creates a boundary layer that is more adiabatic than it would be otherwise, another cause of discrepancy between the simulation and that observed.

3.5 Initialization Sensitivity

Model initialization, or the date and time at which a simulation starts, while inconsequential in modeling quiescent, summertime periods, may play an important role in modeling CAPs. The NAM reanalysis meteorological grids used to initialize WRF often inaccurately capture the thermodynamic structure of the boundary layer during CAPs, which stems from limitations of the data assimilation scheme.

In order to examine the sensitivity of the model simulations to the initial atmospheric state, two additional model runs were performed: DEC30 and JAN01, initialized 30 December 2010 (one day before BASE) and 1 January 2011 (one day after BASE), respectively. The time series of BASE (red), DEC30 (blue), JAN01 (orange), and observations (black) at Syracuse, UT, shown in Fig. 3.7b, suggests there is not much sensitivity of surface temperature to initialization date for this particular CAP episode. Each temperature trace follows a similar trend, and no one exhibits a clear warm or cold bias as compared to the others. Even JAN01, which started with temperatures higher than observations (visible as the orange trace at the left of the plot in Fig. 3.7 b), quickly cooled and was able to capture the diurnal cycle throughout the rest of the event.

Even at Logan, in Cache Valley, which is further away from the influence of the NAM's assimilation of the Salt Lake City rawinsonde, there is no substantive sensitivity in surface air temperature to the date on which the model is initialized. Similarly, no major differences were evident in the Uinta Basin (not shown).

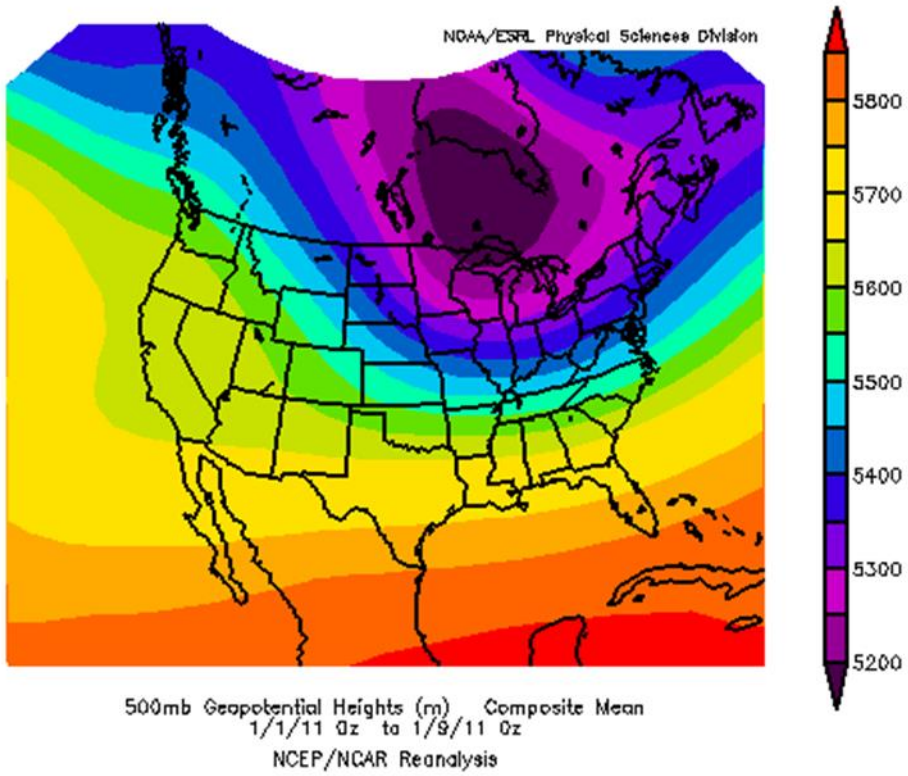

Figure 3.1: Composite average of 500 hPa geopotential height (m) from National Centers for Environmental Prediction (NCEP) North American Regional Reanalyses for the period from 0000 UTC 1 January to 0000 UTC 9 January 2011. Images provided by the NOAA/ESRL Physical Sciences Division, Boulder Colorado (http://www.esrl.noaa.gov/).

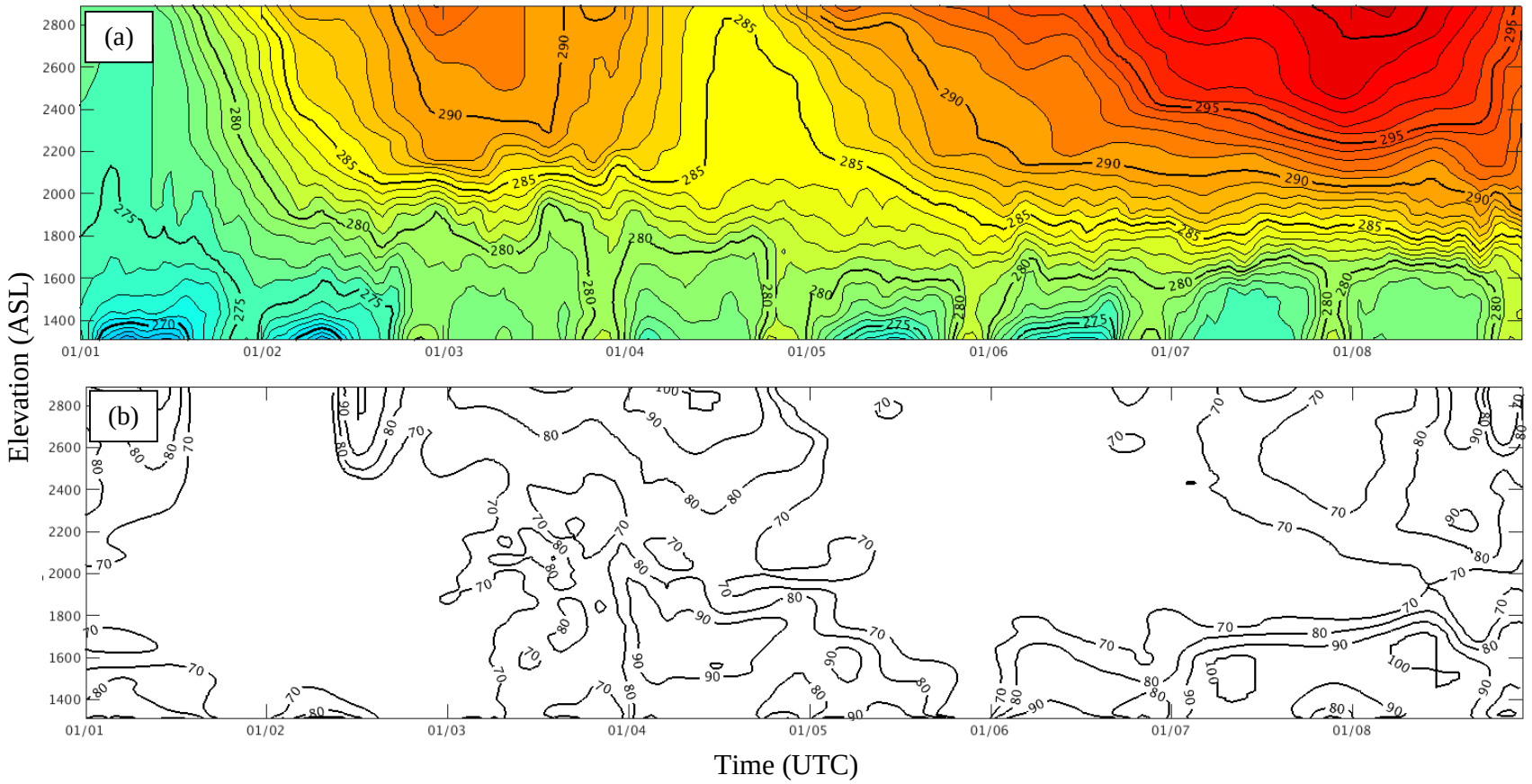

Figure 3.2: Observed conditions at ISS near the center of the SLV from 0000 UTC 1 January 2011 to 0000 UTC 9 January 2011 for: (a) potential temperature (K); (b) relative humidity (%). Data derived from PCAPS resources by Lareau and Horel (2015).

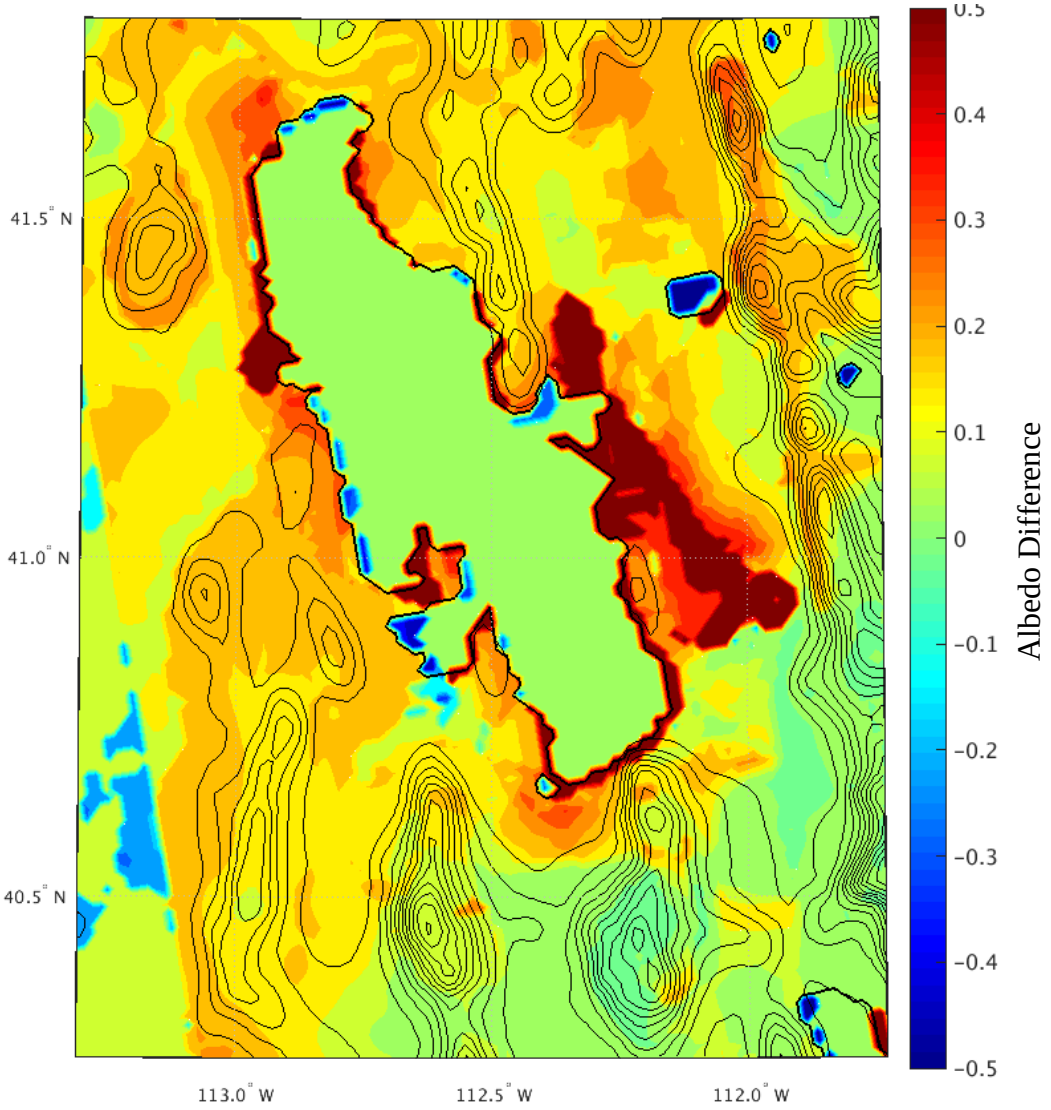

Figure 3.3: Difference in average albedo between BASE and USGS simulations (BASE minus USGS) over the period from 0000 UTC 1 January 2011 to 0000 UTC 9 January 2011. Elevation contoured as solid black lines at an interval of 150 m.

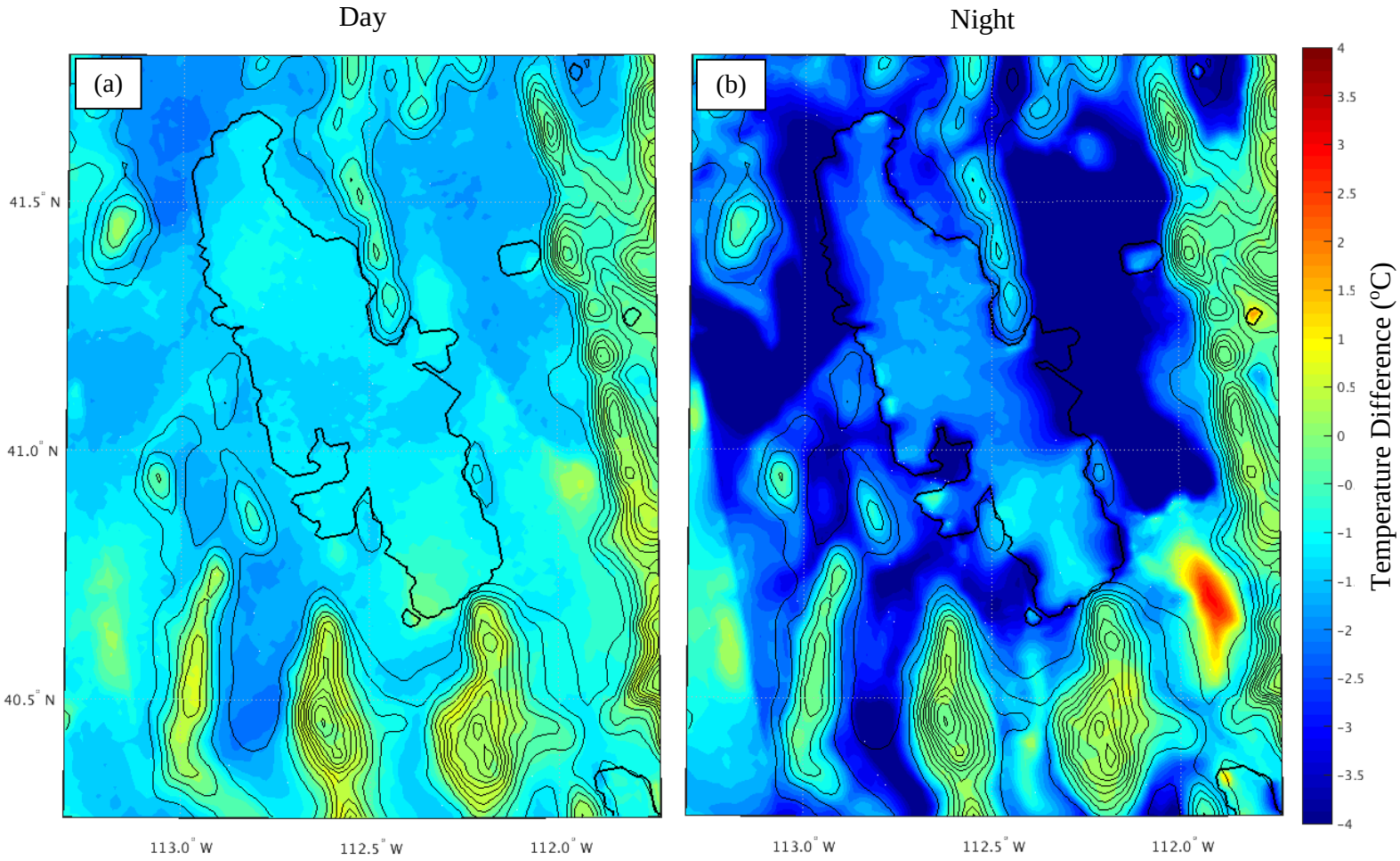

Figure 3.4: Elevation contoured as solid black lines at an interval of 150 m. Difference in average 2 m temperature (°C) between BASE and USGS simulations (BASE minus USGS) over the period from 0000 UTC 1 January 2011 to 0000 UTC 9 January 2011 during: (a) day, 1800 – 0000 UTC; (b) night, 0600 – 1200 UTC.

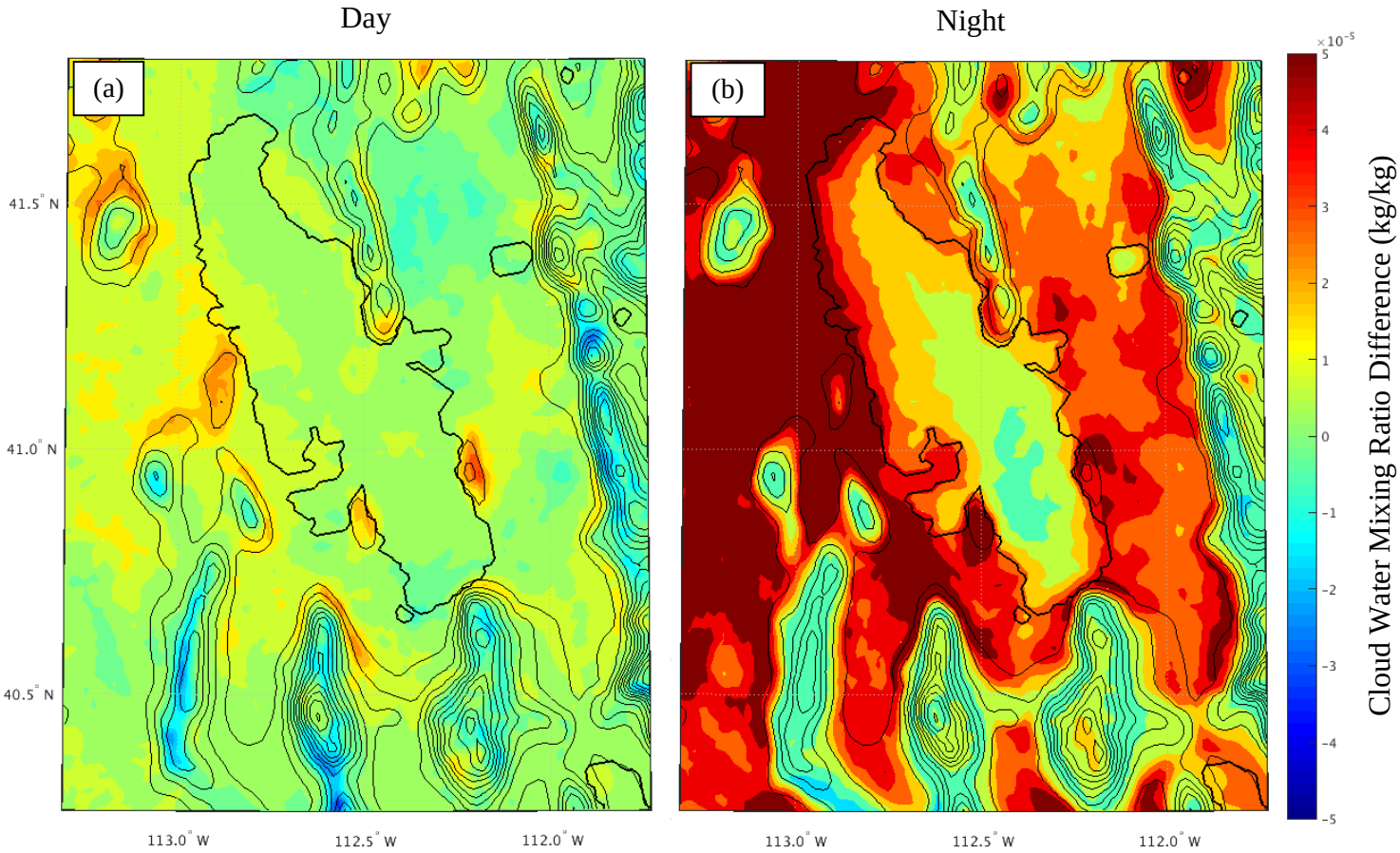

Figure 3.5: Elevation contoured as solid black lines at an interval of 150 m. Difference in average cloud water mixing ratio (kg/kg) in first ten model levels between BASE and USGS simulations (BASE minus USGS) over the period from 0000 UTC 1 January 2011 to 0000 UTC 9 January 2011 during: (a) day, 1800 – 0000 UTC; (b) night, 0600 – 1200 UTC .

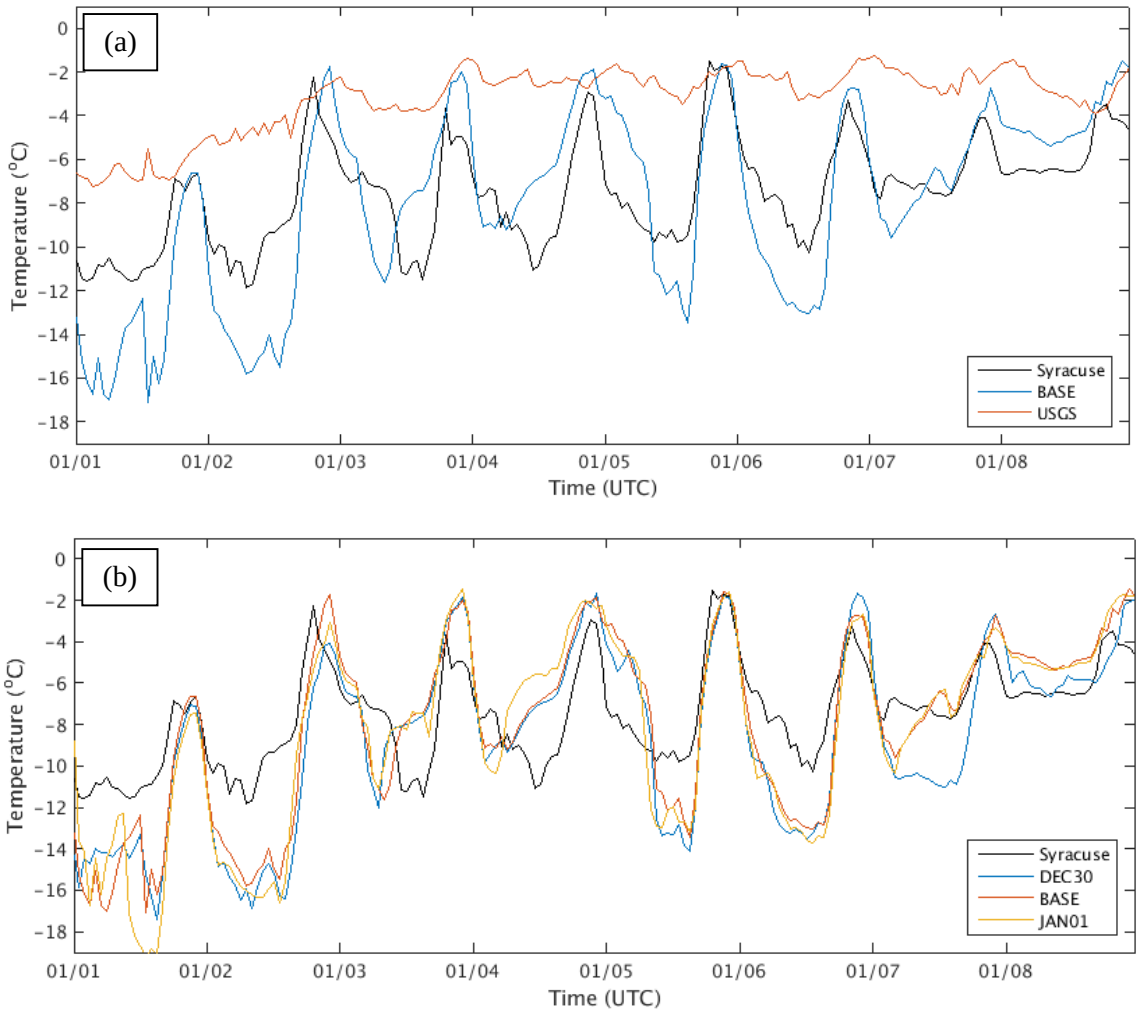

Figure 3.6: Temperature (°C) at Syracuse, UT (QSY) from 0000 UTC 1 January 2011 to 0000 UTC 9 January 2011 for: (a) land use simulations; (b) initialization time simulations.

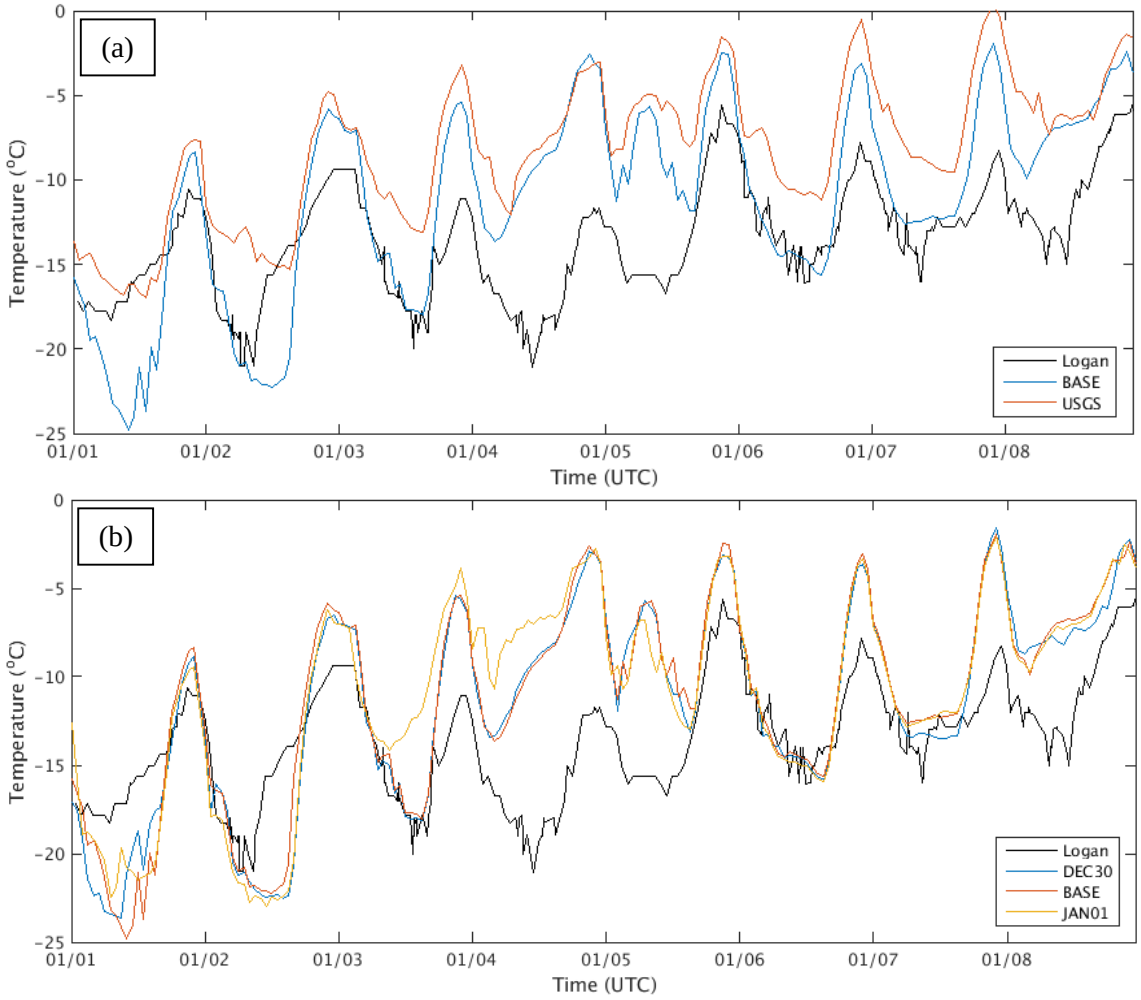

Figure 3.7: Temperature (°C) at Logan, UT (KLGU) from 0000 UTC 1 January 2011 to 0000 UTC 9 January 2011 for: (a) land use simulations; (b) initialization time simulations.

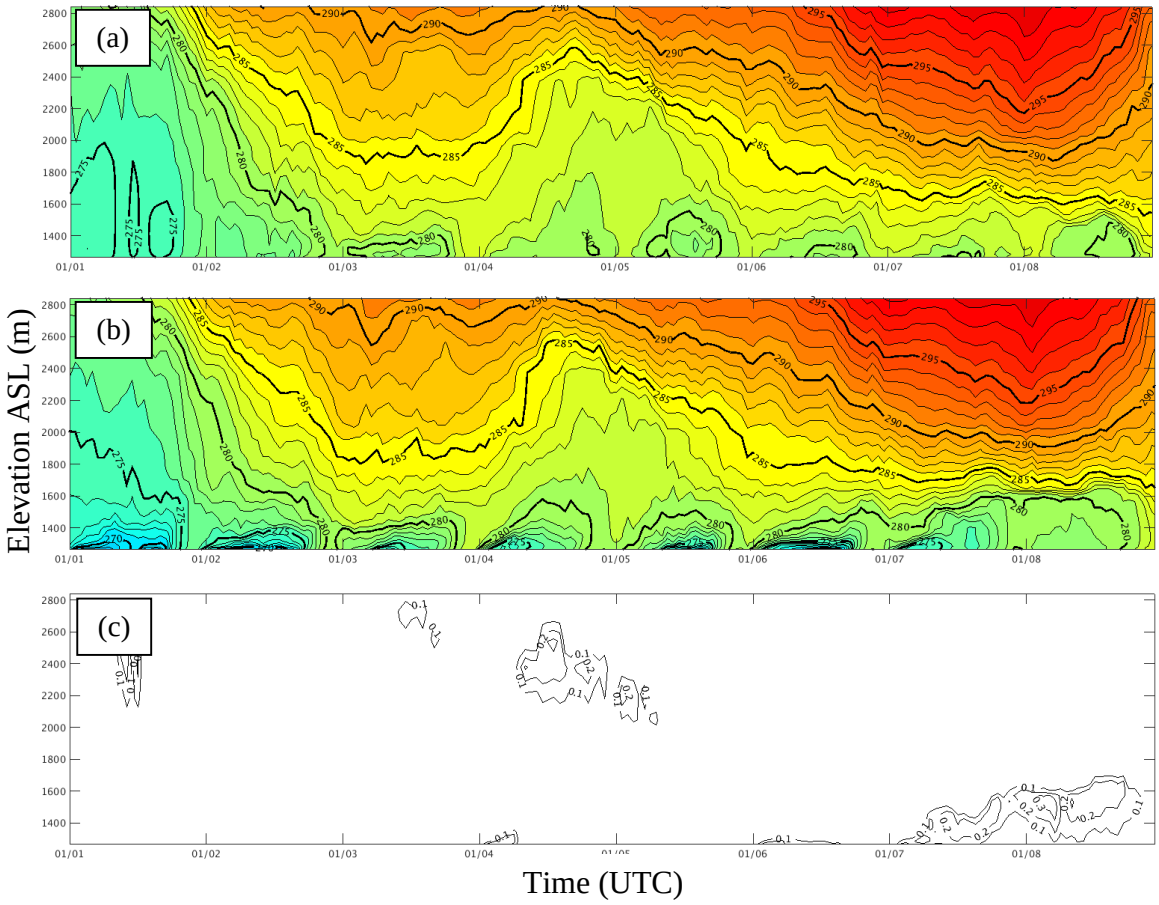

Figure 3.8: Modeled conditions at Syracuse, UT (QSY) from 0000 UTC 1 January 2011 to 0000 UTC 9 January 2011 for: (a) USGS potential temperature (K); (b) as in (a), except for USGS; (c) BASE cloud water mixing ratio (kg/kg).

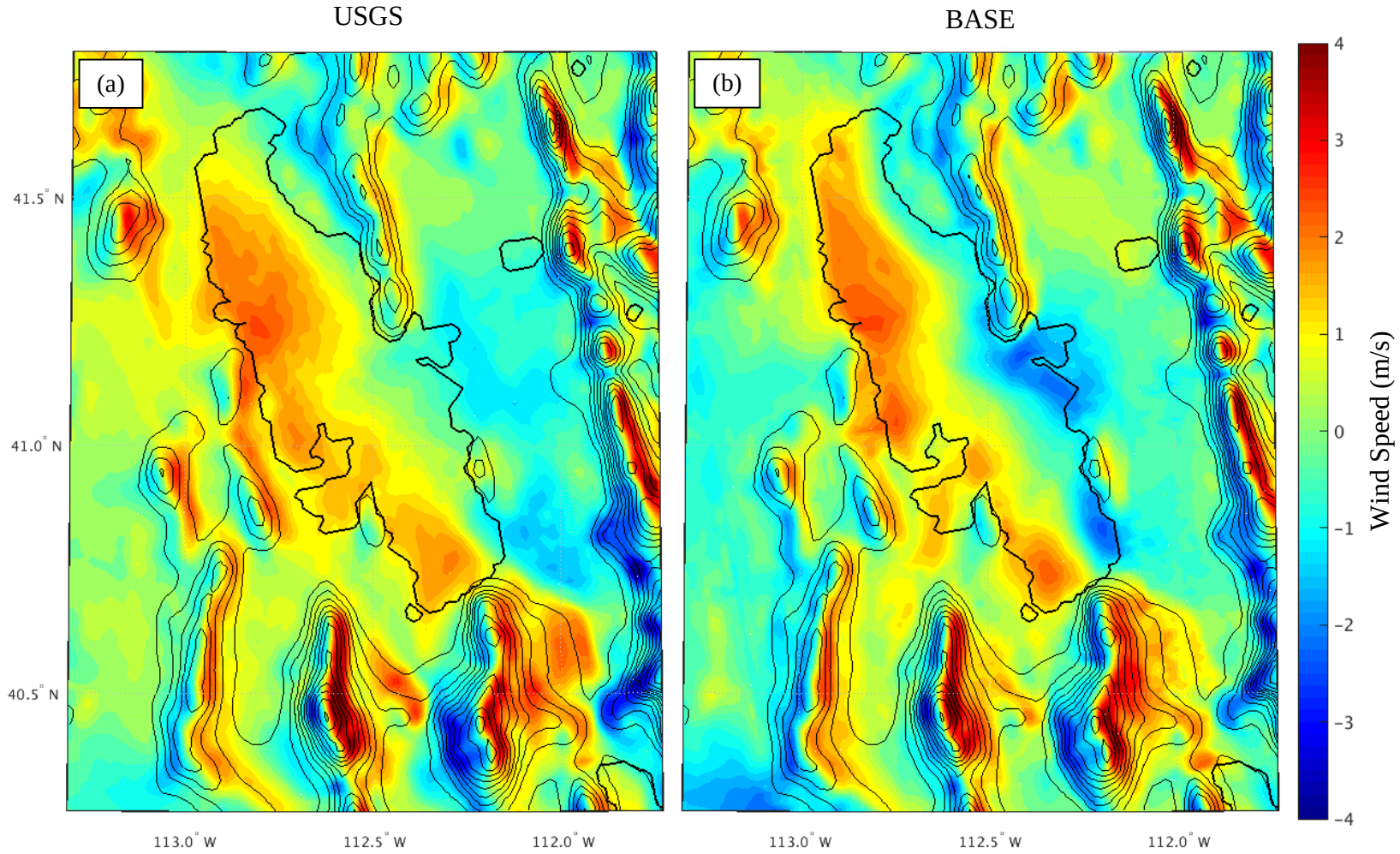

Figure 3.9: Elevation contoured as solid black lines at an interval of 150 m. Average zonal (u) wind (m/s) over the period from 0000 UTC 1 January 2011 to 0000 UTC 9 January 2011 during the nighttime period, 0600 – 1200 UTC for: (a) USGS; (b) BASE.

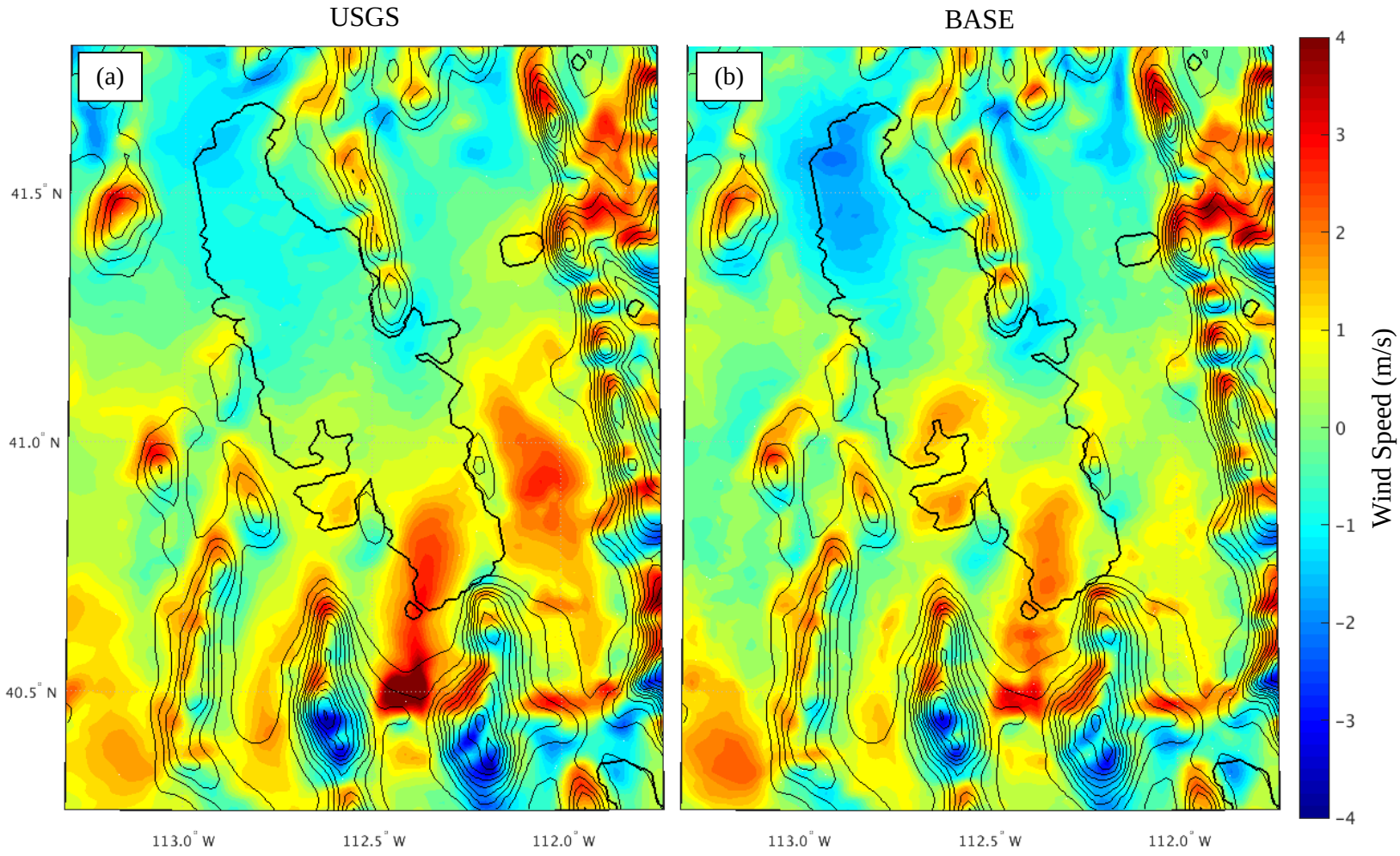

Figure 3.10: Elevation contoured as solid black lines at an interval of 150 m. Average meridional (v) wind (m/s) over the period from 0000 UTC 1 January 2011 to 0000 UTC 9 January 2011 during the nighttime period, 0600 –1200 UTC for: (a) USGS; (b) BASE.

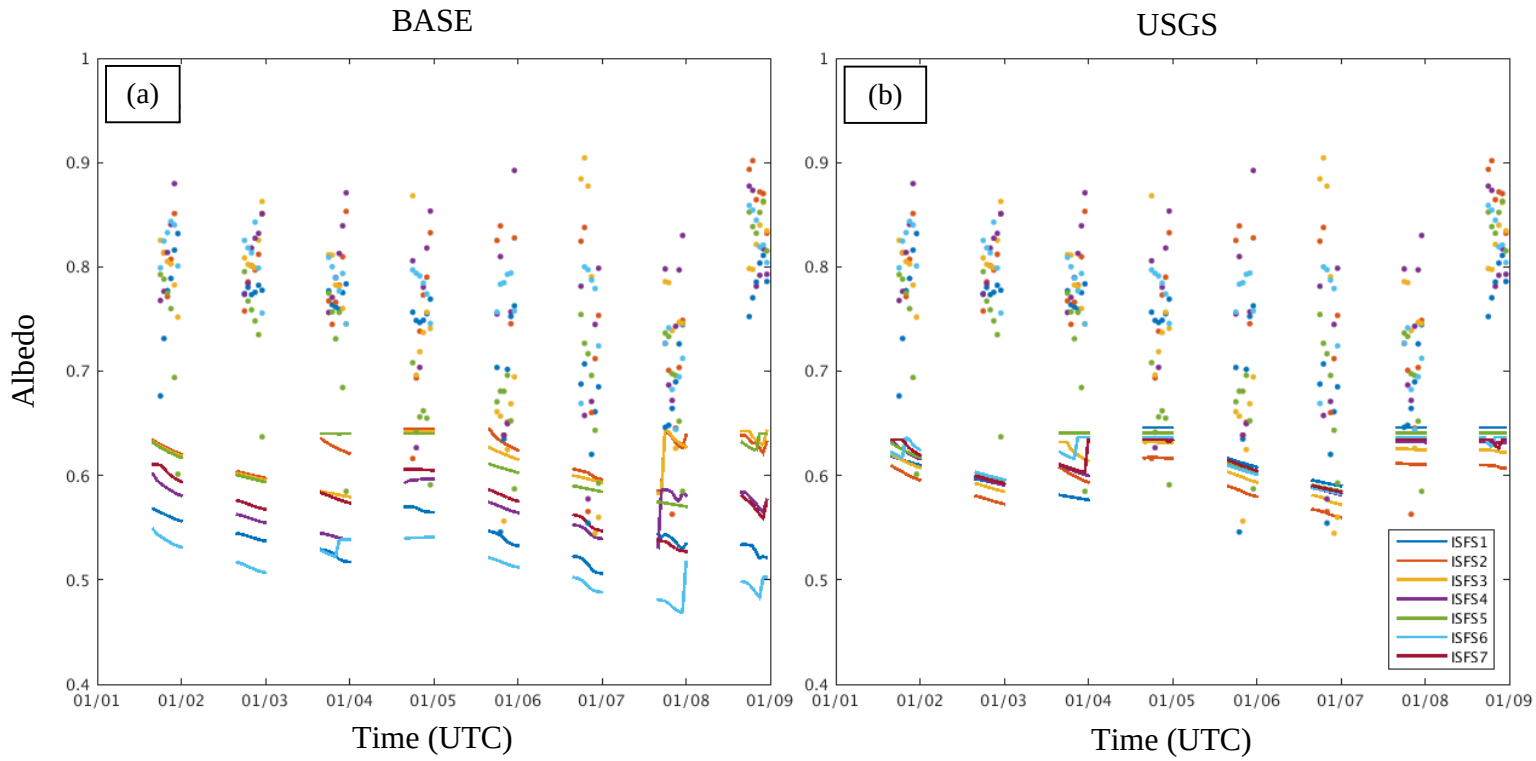

Figure 3.11: Observed (dots) and model (solid lines) albedo from 0000 UTC 31 December 2010 to 0000 UTC 9 January 2011 for: (a) USGS simulation; (b) BASE simulation. Colors correspond to each station, as defined by figure legend.

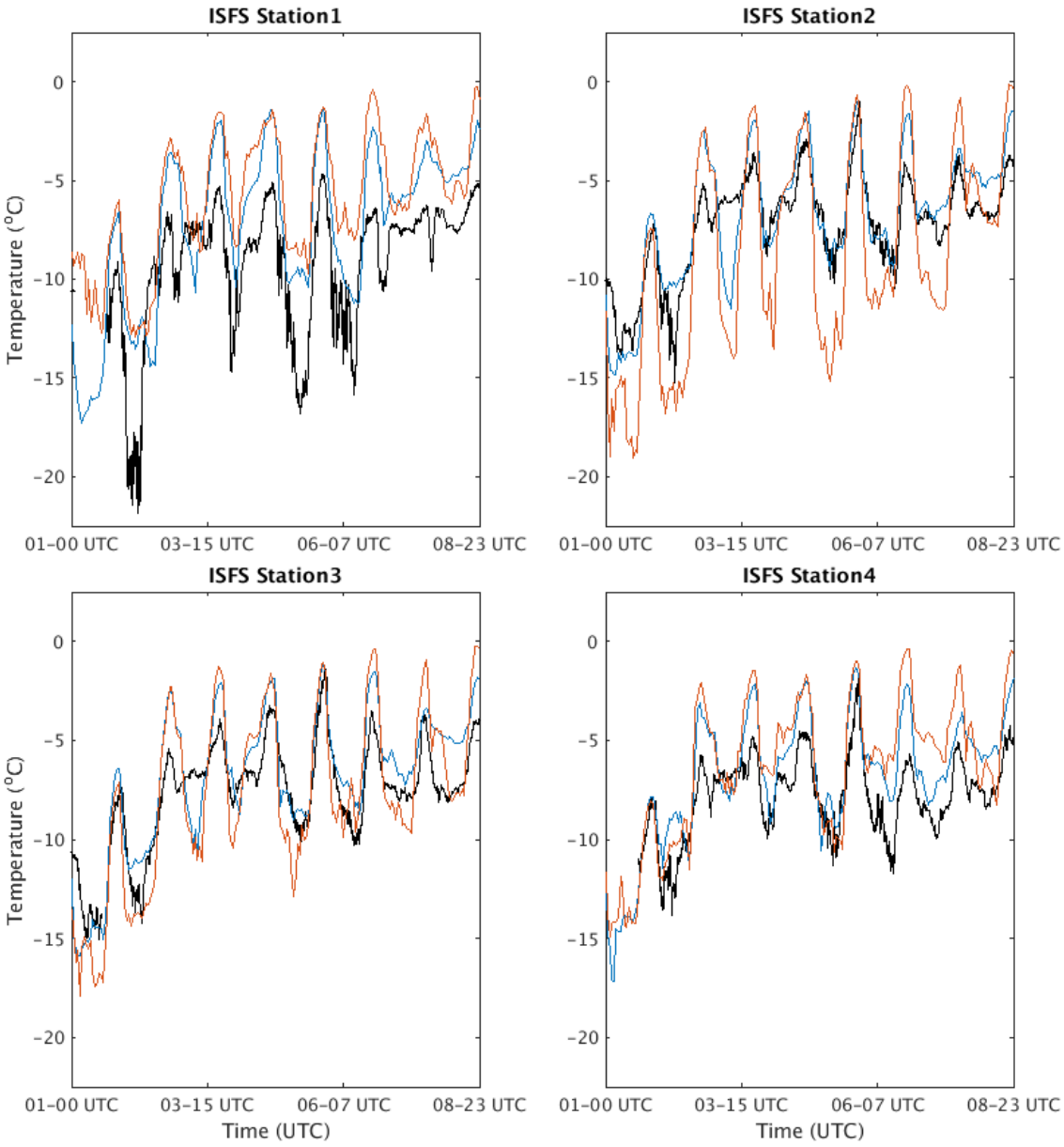

Figure 3.12: Temperature (°C) at the seven ISFS sites from 0000 UTC 1 January 2011 to 0000 UTC 9 January 2011, as labeled (day-time UTC). Observations (black), BASE simulation (blue), USGS simulation (red).

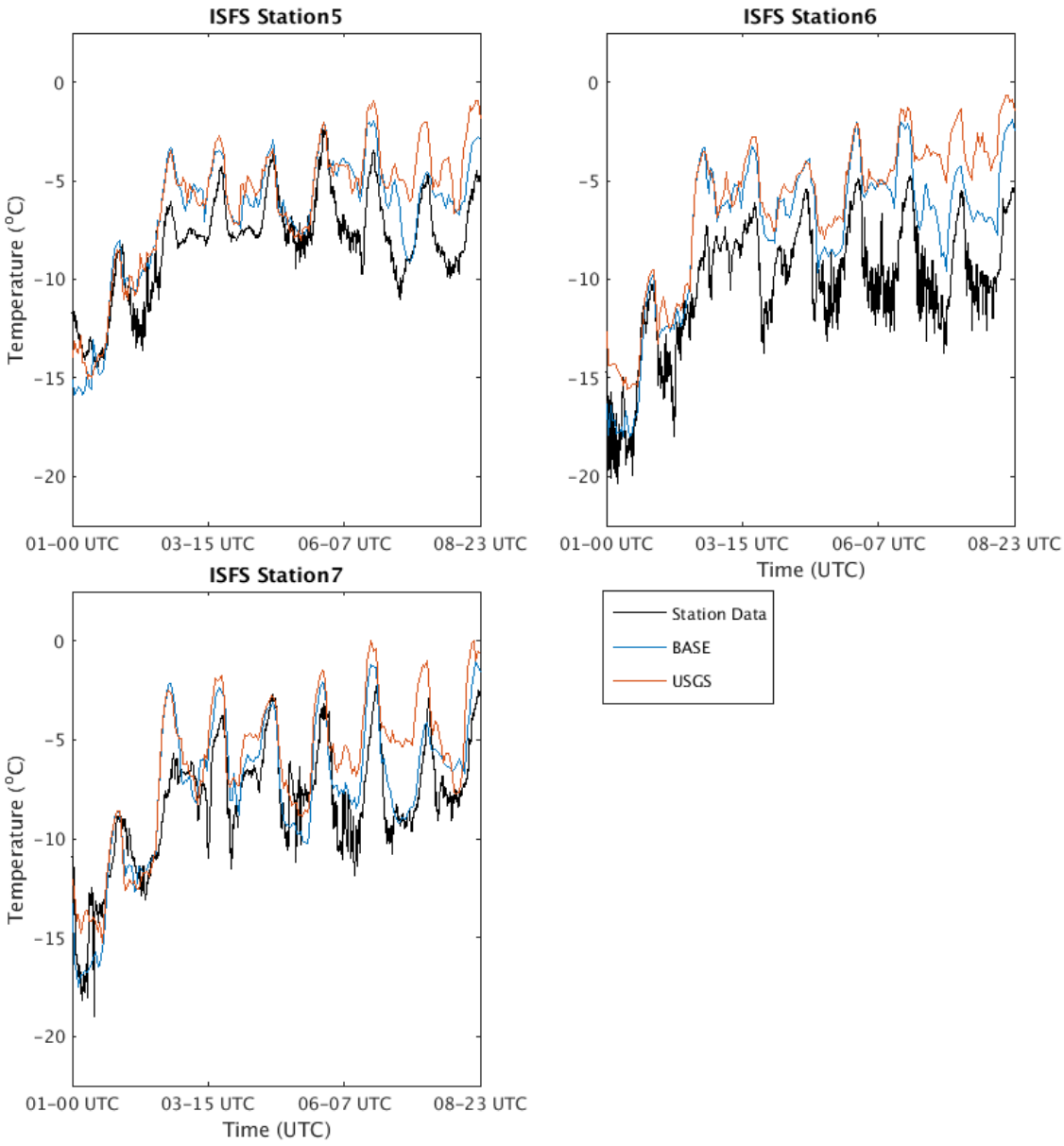

Figure 3.12: Continued.

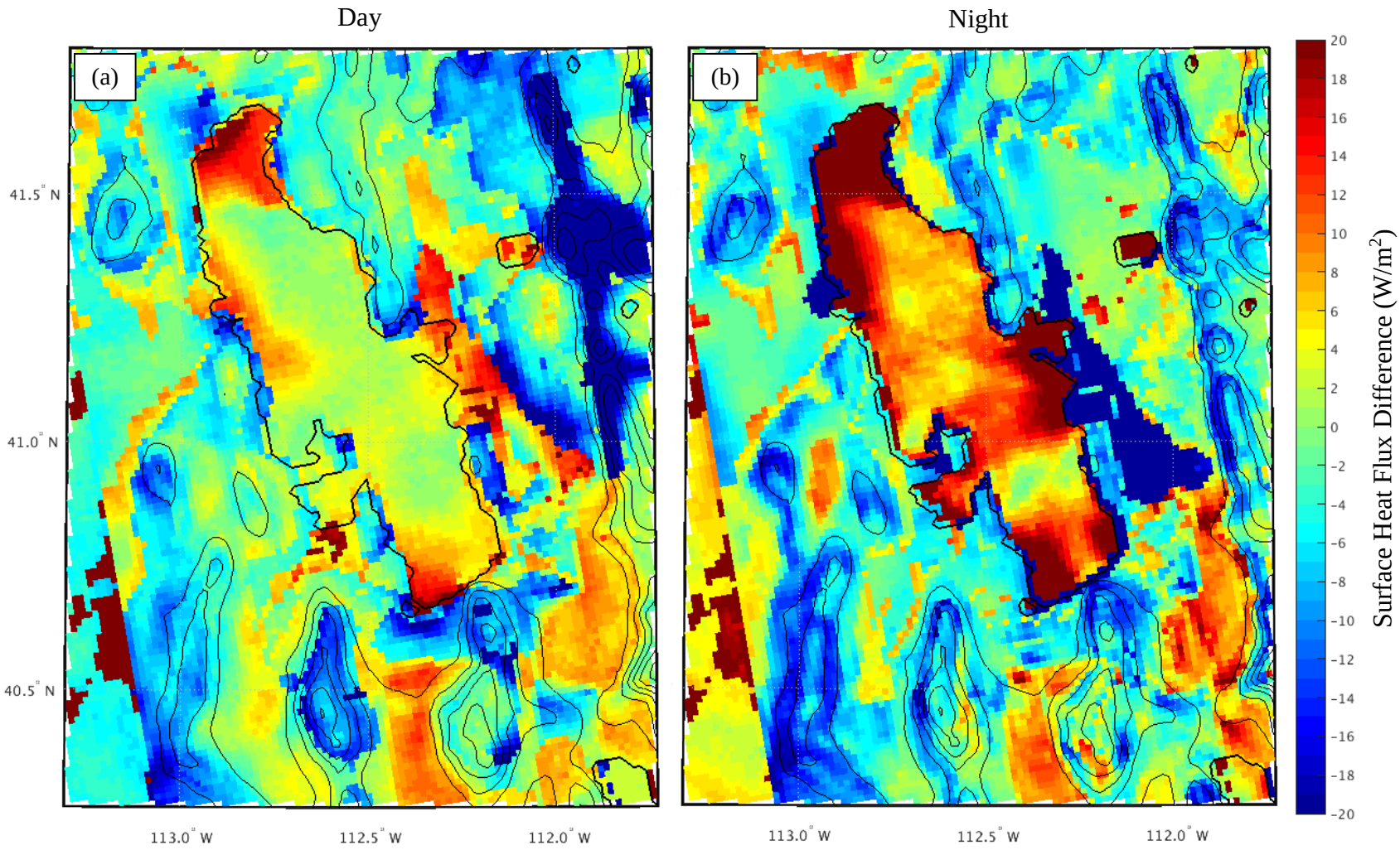

Figure 3.13: Elevation contoured as solid black lines at an interval of 250 m. Difference in surface heat flux (W/m^2) between BASE and USGS simulations (BASE minus USGS) over the period from 0000 UTC 1 January 2011 to 0000 UTC 9 January 2011 during: (a) day, 1800 – 0000 UTC; (b) night, 0600 – 1200 UTC .

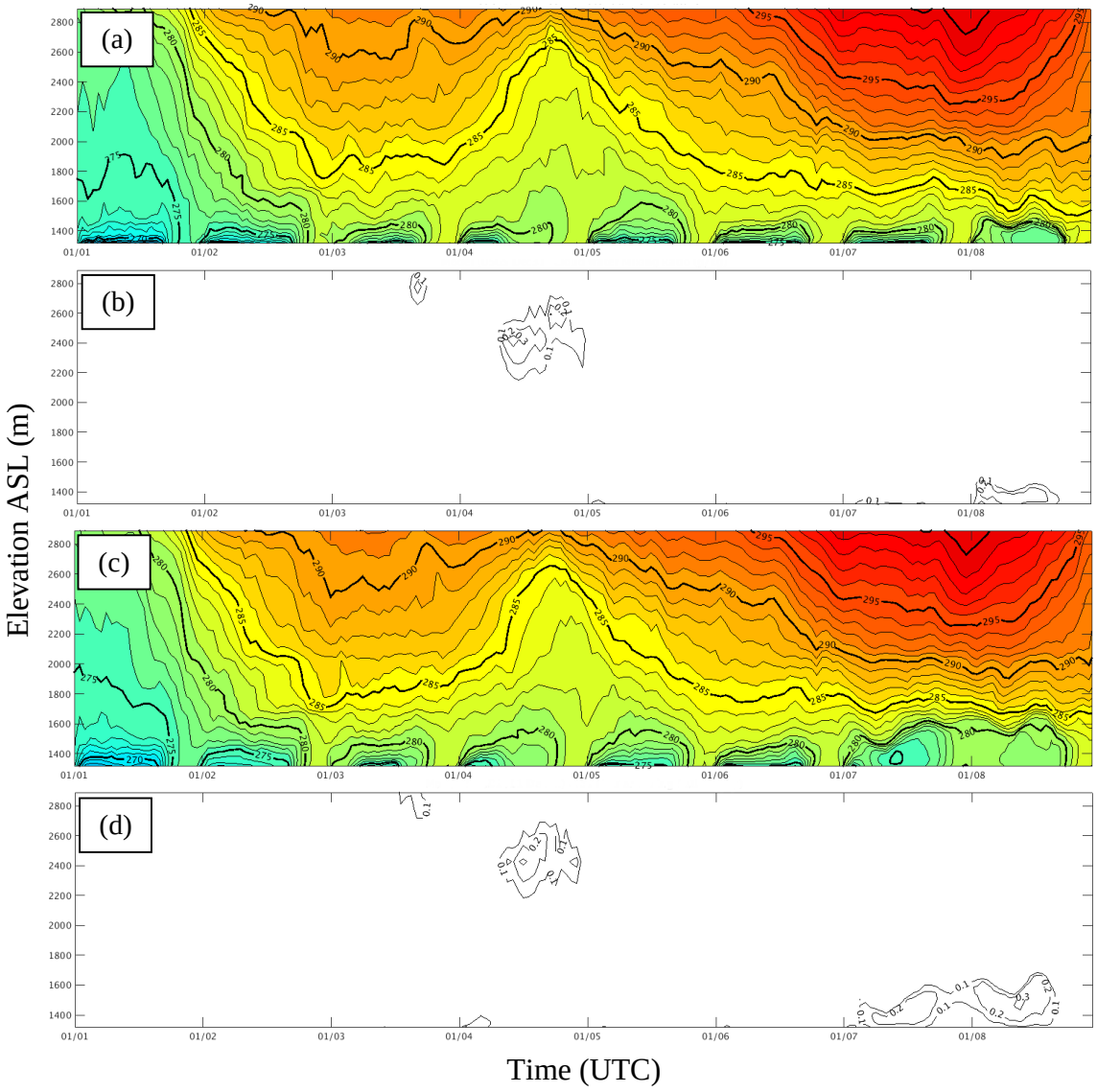

Figure 3.14: Modeled conditions in the SLV from 0000 UTC 1 January 2011 to 0000 UTC 9 January 2011 for: (a) USGS potential temperature (K); (b) USGS cloud water mixing ratio (g/kg); (c) as in (a), except for BASE; (d) as in (b), except for BASE.

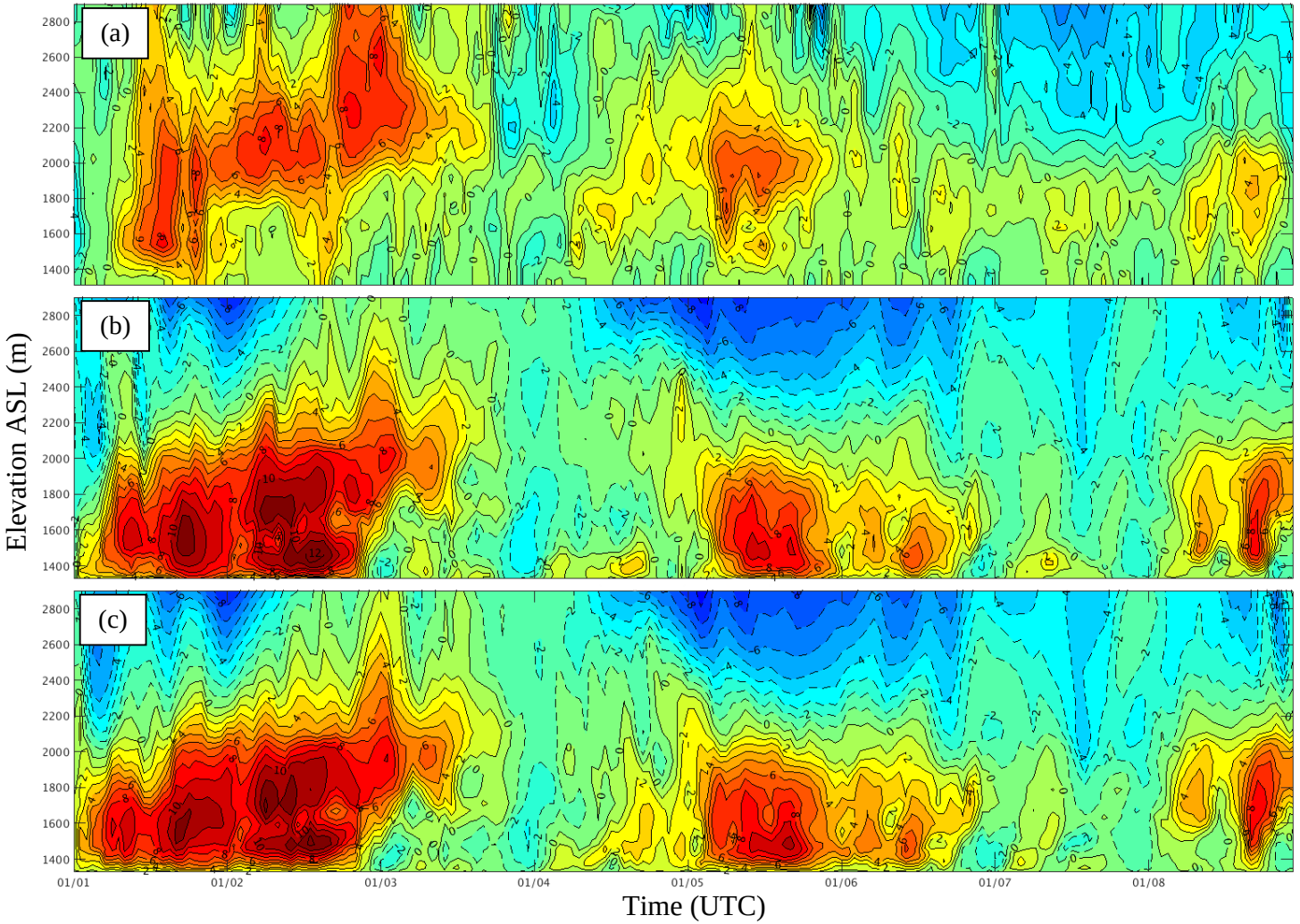

Figure 3.15: Meridional (v) wind component (m/s) in the central SLV from 0000 UTC 1 January 2011 to 0000 UTC 9 January 2011 for: (a) observation; (b) USGS; (c) BASE.

CHAPTER 4

CONCLUSIONS AND DISCUSSION

4.1 Overview and Research Questions

Numerical sensitivity simulations were conducted to investigate the impact of changes in static land use, snow and atmospheric initialization fields, and dynamic land cover parameterizations on the simulation of a CAP in northern Utah from 1-8 January 2011. The shallow nature of the cold pool boundary-layer results in a heightened sensitivity to changes in these model parameters during persistent CAPs, and illustrates the importance of properly specifying surface state in CAP simulations. The fundamental issues that served as the basis for this modeling study were 1) the outdated and/or unrepresentative land use classification schemes utilized by the WRF model, 2) the poor model initialization of snow cover fields, and 3) inadequate parameterization of land surface and snow cover interactions. The USGS dataset, normally the default within WRF's namelist options, uses data retrieved from AVHRR satellites in 1992 and 1993. Because of this, much of the Salt Lake Basin's land cover is incorrectly classified, including most of the now heavily urbanized SLV. In addition, the areal extent of the GSL is much larger than that observed during recent years.

Partial answers to the specific research questions posed in Chapter 1 and additional related discussions on the implications of these findings are now provided.

- *Does improved treatment of WRF model parameterizations of land use, land cover, and surface albedo affect sensible weather fields at the surface and aloft?*

The differences between the BASE and USGS numerical simulations for the 1-8 January 2011 CAP shown in Chapter 3 highlight the sensitivity to differences in static land use and dynamic land cover. The incorrect specification of the areal extent of the GSL in the USGS land use dataset contributes to higher temperatures and a damped diurnal temperature cycle at sites, such as Syracuse, UT, located close to the Lake. Improved specification of the areal extent of the Lake by modifying the NLCD 2011 land use dataset as well as improved treatment of albedo and snow cover led to better simulations of the temporal evolution of surface air temperature during the CAP. Thermally-driven flows and the vertical static stability in the lowest 300 m of the boundary-layer, which are two factors critical for pollutant dispersion and transport near the surface during CAPs, were also sensitive to changes in the static land use and dynamic land cover. Simulated cloud cover during the end of the CAP was also sensitive to changes in the static land use and dynamic land cover, with a more realistic build-up of low clouds and fog observed in the BASE simulation during 6-8 January 2011 compared to the USGS case.

- *Does improved specification of snow cover and snow water equivalent fields in the model lead to closer correspondence of the model simulations to the conditions observed?*

NAM reanalysis fields of snow cover and snow water equivalent were used to initialize the USGS model run while observations were used to crudely adjust the amount of snow as a function of elevation in the BASE simulation. Physically-realistic responses to the snow initialization changes were seen in the temperature, wind, and cloud

cover/moisture fields. For example, the combination of specifying unrealistically deep snowpack in the SLV and too much lake surface to its north in USGS led to stronger nocturnal down valley/land breezes compared to BASE. Increasing the snow cover throughout the regions surrounding the Lake in BASE relative to USGS resulted in a widespread increase in albedo with localized decreases where snow depth was decreased. Increasing albedo likely contributed to lower temperatures near the surface and increased stability in the boundary layer surrounding the Lake in the BASE simulation. Comparison of the two model simulations to observations in the SLV indicated that the cumulative changes in snow cover and land use tended to improve the temporal evolution of 2-m air temperature and boundary layer potential temperature and moisture fields in BASE relative to USGS.

The implementation of the NLCD 2011 land use data ultimately improved model performance in areas where the USGS land use data were severely outdated, such as the increasingly urbanized SLV and near the GSL. NLCD 2011 also has the advantage of four unique urban classifications, which allows for better interaction between snowfall and the land surface, and thus albedo. However, when more closely examining the physical difference between the four urban classifications, it was found that roughness length was the only parameter altered between them, which has an impact on flow patterns and pollutant transport, but not albedo. In fact, the maximum albedo attainable by these land use classifications, as well as others, was far lower than albedos that were observed during the PCAPS field campaign. As a result, the interactions between snow cover and land use underrepresented albedos within the valley, even after adjusting parameters within the model.

- *To what extent are the model simulations for this case sensitive to the timing of the initialization of the model?*

Altering the start date of the model simulation over the 3-day period from 30 December 2010 to 1 January 2011 did not noticeably affect the simulation of the CAP during the subsequent period from 1-8 January 2011. Comparing surface air temperature trends and spatial averages of temperature, moisture, and wind variables revealed no major differences between these simulations. It was hypothesized at the outset of this study that poor initialization of the shallow CAP by the NAM would affect the subsequent evolution of the model simulations. However, it appears in this case that the initial fields were close enough to those observed over this 3-day span that the model was more sensitive to the underlying terrain and specification of surface state. A more comprehensive analysis using additional CAPS with differing characteristics and initialization errors would be required to ascertain more completely the sensitivity to the initial atmospheric state.

Based on the answers to the main research questions posed by this study, its key findings are the following:

- This study represents the most comprehensive evaluation to date of a numerical simulation of a wintertime CAP simulation in Utah's heavily urbanized SLV and shows that a WRF numerical simulation with appropriate land surface specification can reproduce the primary features of a wintertime persistent CAP episode.
- The intensity, cloud cover, vertical structure, and boundary-layer flows within the SLV CAP below ~300 m AGL are heavily influenced by the numerical treatment of land use and snow cover.
- The CAP characteristics are not highly sensitive to variations in initialization time

for this particular CAP episode.

The differences between the simulations resulting from their sensitivity to the underlying surface conditions have implications for the modeling work currently underway at the Utah DAQ that is required to assess emission control strategies as part of State Implementation Plans. Realistic atmospheric model simulations are required to drive the air chemistry model simulations. Inaccurate treatment of the surface state in atmospheric models may lead to inaccurate boundary layer depths and horizontal and vertical advection of pollutants that might affect the sensitivity of air chemistry models to the emission control strategies being tested.

The evaluation of the numerical simulations relative to PCAPs observations highlight several model shortcomings that should be addressed. These limitations could be overcome by:

- Ongoing (at least seasonally) updating of land use and areal extents of shallow lakes.
- Improved snow analyses for shallow, rapidly evolving snow cover using a combination of satellite and in situ data.
- More sophisticated representation of the effects of snow cover for urban areas.
- Improved parameterization of snow albedo as a function of snow age and underlying land use within the Noah land surface model.
- Improved planetary boundary layer treatment of vertical diffusion and mixing in stable boundary layers.

REFERENCES

Alcott, T. I. and W. J. Steenburgh, 2013: Orographic influences on a Great Salt Lake-effect snowstorm. *Mon. Wea. Rev*., **141**, 2432–2450.

Baker, K. R., H. Simon, and J. T. Kelly, 2011: Challenges to modeling "cold pool" meteorology associated with high pollution episodes. *Env. Sci. and Tech.*, **45**, 7118-7119.

Baklanov, A. A., B. Grisogono, R. Bornstein, L. Mahrt, S. S. Zilitinkevich, P. Taylor, S. E. Larsen, M. W. Rotach, and H. J. S. Fernando, 2011: The nature, theory, and modeling of atmospheric planetary boundary layers. *Bull. Amer. Meteor. Soc*., **92**, 123–128.

Billings, B. J., V. Grubišić, and R. D. Borys, 2006: Maintenance of a mountain valley cold pool: a numerical study. *Mon. Wea. Rev.*, **134**, 2266–2278.

Blazquez, J., N. L. Pessacg, and P. L. M. Gonzalez, 2013: Simulation of a baroclinic wave with the WRF regional conditions in an ideal and a real experiment. *Met. Apps.*, **20**, 447–456.

Chen, F., M. Barlage, M. Tewari, R. Rasmussen, J. Jin, D. Lettenmaier, B. Livneh, C. Lin, G. Miguez-Macho, G. Y. Niu, L. Wen, and Z. L. Yang, 2014: Modeling seasonal snowpack evolution in the complex terrain and forested Colorado Headwaters region: a model intercomparison study. *J. Geophys. Res. Atmos*., **119**, 13,795–13,819.

Cheng, F., Y. Hsu, and P. Lin, 2013: Investigation of the effects of different land use and land cover patterns on mesoscale meteorological simulations in the Taiwan area. *J. Appl. Meteor. and Climate*, **52**, 570-587.

Fry, J. A., G. Xian, S. Jin, J. A. Dewitz, C. G. Homer, L. Yang, C. A. Barnes, N. D. Herold, and J. D. Wickham, 2011: Completion of the 2006 National Land Cover Database for the conterminous United States. *Photogram. Eng. and Rem. Sensing*, **77**, 855-864.

Gallus, W. A. and J. F. Bresch, 2006: Comparison of impacts of WRF dynamic core, physics package, and initial conditions on warm season rainfall forecasts. *Mon. Wea. Rev.*, **134**, 2632-2641.

Grim, J. A., J. C. Knievel, and E. T. Crosman, 2013: Techniques for using MODIS data to remotely sense lake water surface temperatures. *J. Atmos. Oceanic Technol*., **30**, 2434–2451.

Holtslag, A. A. M., G. Svensson, P. Baas, S. Basu, B. Beare, A. C. M. Beljaars, F. C. Bosveld, J. Cuxart, J. Lindvall, G. J. Steeneveld, M. Tjernström, and B. J. H. Van De Wiel, 2013: Stable atmospheric boundary layers and diurnal cycles: challenges for weather and climate models. *Bull. Amer. Meteor. Soc*., **94**, 1691–1706.

Jin, S., L. Yang, P. Danielson, C. Homer, J. Fry, and G. Xian, 2013: A comprehensive change detection method for updating the National Land Cover Database to circa 2011. *Rem. Sensing of Env*., **132**, 159-175.

Kain, J. S., 2004: The Kain–Fritsch convective parameterization: an update. *J. Appl. Meteor*., **43**, 170–181.

Lareau, N. P., E. Crossman, C. D. Whiteman, J. Horel, S. Hoch, W. Brown, and T. Horst, 2013: The Persistent Cold-Air Pool Study. *Bull. Amer. Meteor. Soc*., **94**, 51-63.

Lareau, N. P. and J. Horel, 2015: Dynamically induced displacements of a persistent cold-air pool. *Boundary-Layer Meteor.*, **154**, 291-316.

Lu, W., Z. Pu, and S. Wang, 2013: Numerical simulation of the life cycle of a persistent wintertime inversion over Salt Lake City. *Boundary-Layer Meteor.*, **148**, 399-418.

Lu, W. and S. Zhong, 2014: A numerical study of a persistent cold-air pool episode in the Salt Lake Valley, Utah. *J. Geophys. Res.*, **199**, 1733-1752.

Neemann, E. M., E. Crosman, J. Horel, and L. Avey, 2014: Simulations of a cold-air pool associated with elevated wintertime ozone in the Uinta Basin, Utah. *ACPD*, **14,** 1-48.

Pinto, J. O., D. B. Parsons, W. O. J. Brown, S. Cohn, N. Chamberlain, and B. Morley, 2006: Coevolution of down-valley flow and the nocturnal boundary layer in complex terrain. *J. Appl. Meteor. Climatol*., **45**, 1429–1449.

Possner, A., E. Zubler, O. Fuhrer, U. Lohmann, and C. Schar, 2014: A case study in modeling low-lying inversions and stratocumulus cloud cover in the Bay of Biscay. *Wea. Forecasting*, **29**, 289-304.

Rakovec, J., J. Merse, S. Jernej, and B. Paradiz, 2002: Turbulent dissipation of the cold-air pool in a basin: comparison of observed and simulated development. *Meteor. Atmos. Phys.*, **79**, 195–213.

Reeves H. D. and D. J. Stensrud, 2009: Synoptic-scale flow and valley cold pool evolution in the western United States. *Wea. Forecasting*, **24**, 1625–1643.

Reeves, H. D., K. L. Elmore, G. S. Manikin, and D. J. Stensrud, 2011: Assessment of forecasts during persistent valley cold pools in the Bonneville Basin by the North American Mesoscale Model. *Wea. Forecasting*, **26**, 447–467.

Saide, P. E., G. R. Carmichael, S. N. Spak, L. Gallardo, A. E. Osses, M. A. Mena-Carrasco, and M. Pagowski, 2011: Forecasting urban PM10 and PM2.5 pollution episodes in very stable nocturnal conditions and complex terrain using WRF-Chem CO tracer model. *Atmos. Env.*, **45**, 2769-2780.

Sertel, E., A. Robock, and C. Ormeci, 2010: Impacts of land cover data quality on regional climate simulations. *Intern. J. of Climatol.*, **30**, 1942-1953.

Silcox, G. D., K. Kelly, E. Crosman, C. D. Whiteman, and B. Allen, 2012: Wintertime PM2.5 concentrations during persistent, multiday cold-air pools in a mountain valley. *Atmos. Env.*, **46**, 17-24.

Whiteman, C. D., X. Bian, and S. Zhong, 1999: Wintertime evolution of the temperature inversion in the Colorado Plateau Basin. *J. Appl. Meteor.*, **38**, 1103-1117.